Environmental Science and Pollution Research (2021) 28:38173–38192
https://doi.org/10.1007/s11356-021-13362-2

RESEARCH ARTICLE

Greenhouse gas emissions (CO_2 and CH_4) and inorganic carbon behavior in an urban highly polluted tropical coastal lagoon (SE, Brazil)

Luiz C. Cotovicz Jr[1,2] · Renato P. Ribeiro[3] · Carolina Ramos Régis[1] · Marcelo Bernardes[1] · Rodrigo Sobrinho[1] · Luciana Oliveira Vidal[4] · Daniel Tremmel[1] · Bastiaan A. Knoppers[1] · Gwenaël Abril[1,5]

Received: 6 September 2020 / Accepted: 4 March 2021 / Published online: 16 March 2021

Abstract

Increasing eutrophication of coastal waters generates disturbances in greenhouse gas (GHG) concentrations and emissions to the atmosphere that are still poorly documented, particularly in the tropics. Here, we investigated the concentrations and diffusive fluxes of carbon dioxide (CO_2) and methane (CH_4) in the urban-dominated Jacarepagua Lagoon Complex (JLC) in Southeastern Brazil. This lagoonal complex receives highly polluted freshwater and shows frequent occurrences of anoxia and hypoxia and dense phytoplankton blooms. Between 2017 and 2018, four spatial surveys were performed (dry and wet conditions), with sampling in the river waters that drain the urban watershed and in the lagoon waters with increasing salinities. Strong oxygen depletion was found in the rivers, associated with extremely high values of partial pressure of CO_2 (pCO_2; up to 20,417 ppmv) and CH_4 concentrations (up to 288,572 nmol L^{-1}). These high GHG concentrations are attributed to organic matter degradation from untreated domestic effluents mediated by aerobic and anaerobic processes, with concomitant production of total alkalinity (TA) and dissolved inorganic carbon (DIC). In the lagoon, GHG concentrations decreased mainly due to dilution with seawater and degassing. In addition, the phytoplankton growth and CH_4 oxidation apparently consumed some CO_2 and CH_4, respectively. TA concentrations showed a marked minimum at salinity of ~20 compared to the two freshwater and marine end members, indicating processes of re-oxidation of inorganic reduced species from the low-salinity region, such as ammonia, iron, and/or sulfides. Diffusive emissions of gases from the entire lagoon ranged from 22 to 48 mmol C m^{-2} d^{-1} for CO_2 and from 2.2 to 16.5 mmol C m^{-2} d^{-1} for CH_4. This later value is among the highest documented in coastal waters. In terms of global warming

Highlights

- Oxygen-depleted river waters were associated with high concentrations of TA and DIC.
- TA and DIC decreased in the mixing region due to re-oxidation processes.
- Extreme high concentrations and emissions of CO_2 and CH_4 were found in hypoxic/anoxic polluted river waters.
- Concentrations and emissions of GHGs decreased seaward as a result of mixing, degassing, and biological uptake.
- The diffusive CH_4 emissions were more important than CO_2 emissions in terms of global warming potential.

Responsible editor: V. V.S.S. Sarma

✉ Luiz C. Cotovicz, Jr
lccjunior@id.uff.br

[1] Programa de Geoquímica, Universidade Federal Fluminense, Niterói, RJ, Brazil

[2] Instituto de Ciências do Mar, Universidade Federal do Ceará, Fortaleza, CE, Brazil

[3] Centro Experimental de Monitoramento e Mitigação Ambiental (CEMMA), Instituto Federal de Educação, Ciência e Tecnologia do Rio de Janeiro (IFRJ), Nilópolis, RJ, Brasil

[4] Laboratório de Ciências Ambientais, Centro de Biociências e Biotecnologia Universidade Estadual do Norte Fluminense, Campos dos Goytacazes, RJ, Brazil

[5] Biologie des Organismes et Ecosystèmes Aquatiques (BOREA), UMR 7208, Muséum National d'Histoire Naturelle, CNRS, IRD, SU, UCN, UA, Paris, France

potential (GWP) and CO_2 equivalent emissions (CO_2-eq), the diffusive emissions of CH_4 were higher than those of CO_2. These results highlight that highly polluted coastal ecosystems are hotspots of GHG emissions to the atmosphere, which may become increasingly significant in future global carbon budgets.

Keywords Carbon dioxide · Methane · Carbonate chemistry · Coastal eutrophication · Environment pollution · Coastal lagoons

Introduction

Coastal eutrophication is one of the major environmental threats to coastal ecosystems worldwide and particularly accelerated and severe in densely populated ecosystems (Nixon 1995; Cloern 2001, Bricker et al. 2008). At advanced stages of eutrophication, the high nutrient and organic matter enrichment lead to profound changes in ecosystem metabolism and biogeochemical cycling, deteriorating the ecological health and water quality. Some adverse effects include occurrence of harmful algal blooms (HABs), acceleration of growth of fungal and bacterial communities, oxygen depletion, and coastal acidification (Bricker et al. 2008; Cai et al. 2011). Studies have suggested that coastal eutrophication has been perturbing the carbon cycling, leading to alteration in carbon budgets and GHG emissions, such as CO_2 and CH_4 (Borges and Abril 2011). CO_2 and CH_4 are the principal well-mixed and long-lived GHGs present in the atmosphere, and, together, these gases answer to more than 80% of the actual increase in the global average atmospheric temperature (IPCC 2013). Global mean atmospheric CO_2 concentrations increased from 280 ppmv during the pre-Industrial Revolution (Siegenthaler et al. 2005) to reach actual concentration overpassing 415 ppmv (NOAA 2019). For CH_4, a more powerful GHG, the concentration changed from 0.72 ppmv in the pre-industrial period (Etheridge et al. 1998) to the current level of about 1.80 ppmv (NOAA 2019). Despite this well-documented atmospheric rise, the sources and sinks of these GHGs in the diverse compartments of the Earth global system are not yet properly understood and quantified, particularly in disturbed coastal ecosystems at subtropical and tropical latitudes.

The low levels of oxygen concentrations in coastal waters are associated with high levels of aquatic partial pressure of CO_2 (pCO_2) enhancing the CO_2 degassing (Frankignoulle et al. 1996, 1998; Borges and Abril 2011) and recently associated with the process of coastal acidification (Cai et al. 2011). In this way, coastal eutrophication can act amplifying the CO_2 emissions by stimulating heterotrophic processes through the respiration of anthropogenic-derived organic carbon (Frankignoulle et al. 1998; Zhai et al. 2007). The internal processes of respiration of organic matter in eutrophic aquatic ecosystems modify not only the CO_2 concentrations but also all the parameters of the carbonate chemistry, with influences on the acid-base properties, altering the pH and concentrations of TA and DIC (Abril and Frankignoulle 2001; Cai et al. 2011; Sunda and Cai 2012; Cotovicz et al. 2018). However, eutrophication can also contribute to promote CO_2 sink by stimulating the primary production with important CO_2 uptake in coastal waters that receive important amounts of nutrients (Borges and Gypens 2010; Cotovicz et al. 2015, 2020; Kubo et al. 2017). In this regard, eutrophication can both amplify CO_2 outgassing (when organic matter is intensely degraded by microbial activities) or CO_2 ingassing (when organic matter is intensely produced by primary producers). These interplays between sources and sinks of CO_2 and alteration in carbonate chemistry depend on local/regional characteristics and are not well-understood.

The anthropogenic-derived CH_4 sources are growing in importance (Reay et al. 2018). The eutrophication is an important driver of aquatic CH_4 emissions to the atmosphere (Beaulieu et al. 2019). Multiple studies in freshwater and brackish waters have found high CH_4 emissions as a result of increase in organic substrate in productive aquatic systems (Nirmal-Rajkumar et al. 2008; Burgos et al. 2015; Cotovicz et al. 2016; Beaulieu et al. 2019). However, some pristine aquatic environments, such as the Congo River, are also important sources of CH_4 to the atmosphere due to the high lateral inputs of carbon from riparian wetlands (flooded forest and aquatic macrophytes; Borges et al. 2019). The production of CH_4 is enhanced in hypoxic and anoxic conditions associated to increased inputs of organic matter to water and sediments. In coastal waters, CH_4 production is most important in low-salinity regions, where methanogenesis is promoted by the low availability of electron acceptors, particularly sulfate (Chanton et al. 1989; Kelley et al. 1990); in high salinity regions, sulfate reduction outcompetes with methanogenesis as the main pathway of sedimentary anaerobic organic matter degradation (Martens and Klump 1980; Martens et al. 1998). In coastal marine sediments with high salinity, large inputs of organic matter are necessary for methanogenesis to occur and generate CH_4-rich gassy sediments (Martens and Klump 1980; Martens et al. 1998). In urbanized coastal regions, the inputs of CO_2 and CH_4 from wastewater treatment plants and untreated domestic effluents are particularly relevant (Nirmal-Rajkumar et al. 2008; Burgos et al. 2015; Cotovicz et al. 2016). This means that regions under influence and/or close to sewage discharge present higher CO_2 and CH_4 concentrations and emissions. In addition, it is important to point that anaerobic respiration processes (such as denitrification, manganese reduction, iron reduction, and sulfate reduction) produce TA and in some cases also involve alteration in DIC concentrations (Abril and Frankignoulle 2001; Rassmann et al. 2020).

Coastal lagoons represent an estuarine typology highly sensitive to develop eutrophication due to the long residence times and due to host large human settlements (Knoppers et al. 1999). These near-shore coastal environments occur in 13% of the world's coastline (Kjerfve 1985), normally exhibiting high levels of primary production (Knoppers et al. 1999). There have been very few studies conducted in coastal lagoons regarding the assessment of concentrations and quantification of emissions of GHGs, particularly in tropical regions (Borges and Abril 2011; Koné et al. 2009, 2010), creating large uncertainties in global GHG budgets. In the present study, we analyze and quantify the concentrations and air-water fluxes of CO_2 and CH_4 in a high-polluted and urban-dominated coastal lagoon, the Jacarepagua Lagoon Complex (JLC), located at the Rio de Janeiro coast (Southeastern, Brazil). The system hosts a population of nearly 1 million of inhabitants along the watershed (Santos Neves et al. 2017). We hypothesized that the strong pollution and eutrophication will contribute with high emissions of GHGs in this system, especially in the riverine waters that receive high loads of organic matter and nutrients from untreated urban effluents (Fig. 1). With this, we constructed a sampling design able to describe the contrasts between riverine and lagoonal conditions by choosing 5 stations in river waters and 5 stations in lagoon waters. Our results showed extremely high concentrations and emissions of CO_2 and CH_4 in anoxic/hypoxic freshwaters. The concentrations and emissions of CO_2 and CH_4 in freshwaters are among the highest documented in coastal waters worldwide and are hotspots of GHG emissions.

Material and methods

Study area

The JLC (Lat. 22°55′ S to 23°03′ S; Long. 43°30′ W to 43°18′ W) is located in the west region of the Rio de Janeiro City

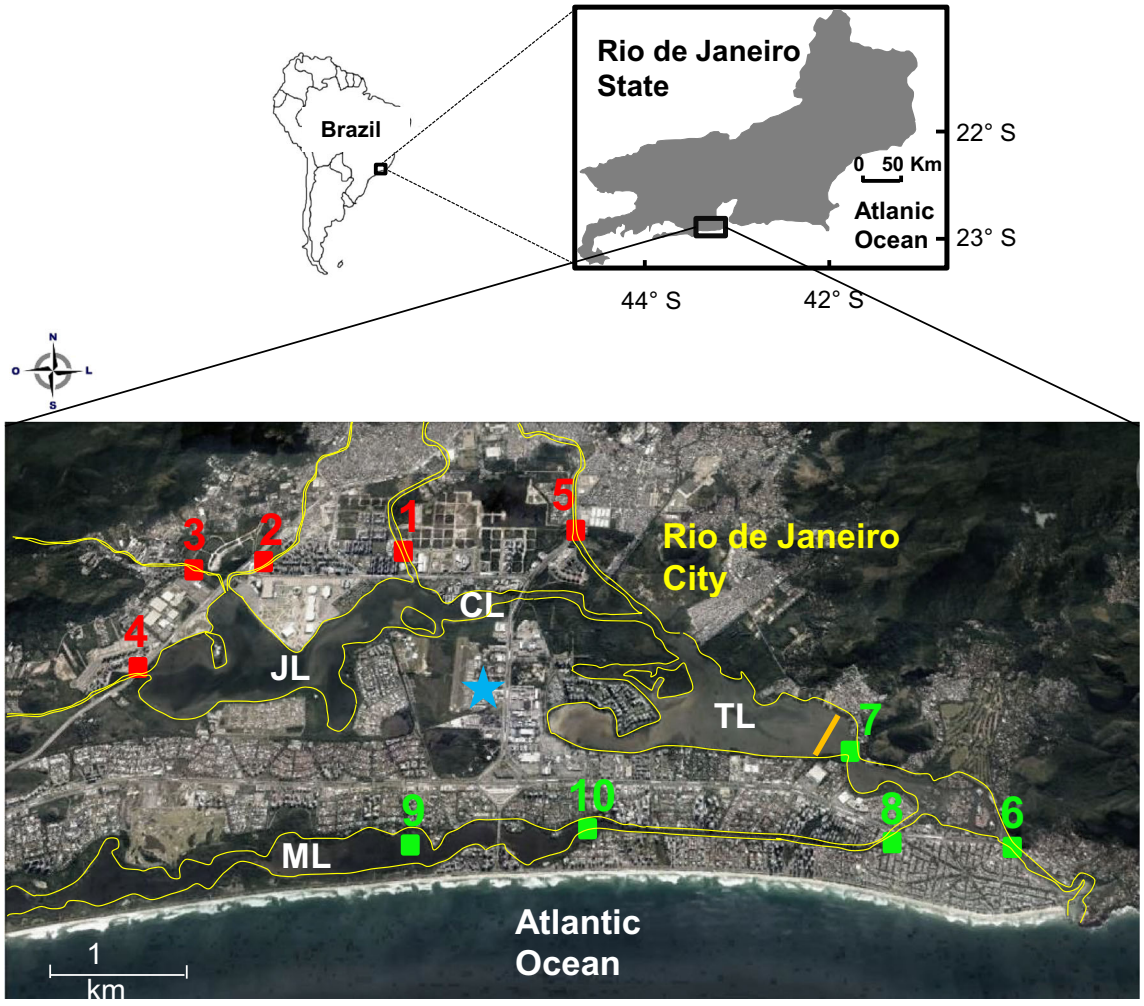

Fig. 1 Map showing the localization of the Jacarepagua Lagoon Complex (JLC). The red squares represent the locations of river stations. The green squares represent the locations of lagoon stations. The blue star represents the location of the meteorological station. The yellow line represents the contour of the lagoons and the rivers. The orange line refers to an ecological barrier that impedes the navigation in the landward direction

(Southeastern Brazil). The system is composed of four coastal lagoons: Jacarepaguá (area = 4.07 km^2), Camorim (A = 0.80 km^2), Tijuca (A=4.34 km^2), and Marapendi (A = 3.33 km^2) (Fig. 1). The total surface area covers about 12.8 km^2, and the drainage basin extends over approximately 280 km^2 (Salloto et al. 2012). The water volume in the lagoon is estimated at about 2.38 × 10^7 m^3 (Sampaio 2008). The annual freshwater inputs to the system are weak, about 3.00 m^3 s^{-1} (Sampaio 2008). However, under strong levels of precipitation, the freshwater inflow can be significantly higher. These lagoons present microtidal amplitude and are enclosured and connected to the sea by only one channel, the Joa Channel (Gomes et al. 2009). The climate in the region is classified as tropical humid, with a wet warm summer and a dry winter (Sampaio 2008). This lagoon complex has been suffering with intense anthropogenic activities developed in its surroundings and along the watershed, mainly urbanization and industrialization (Gomes et al. 2009). Actually, the human population surrounding the JLC is about 1 million of inhabitants, reflecting in high loads of domestic and industrial effluents discharged directly into the water body and its rivers. The wastewater services collection are still very precarious and inefficient, covering less than 60% of the total produced (ANA 2019). Taking account the population of the watershed and the estimates of emissions of effluents per capita (Wallace 2005), the amount of effluents discharges is on the same order of the freshwater inputs to the system (~ 3.4 m^3 s^{-1}), i.e., the mean wastewater volume loaded to the lagoon is almost equivalent to the freshwater river loads. This results in a heavily eutrophication process in this system, with perennial presence of cyanobacterial blooms and frequent episodes of hypoxia/anoxia (Gomes et al. 2009; De-Magalhães et al. 2017).

Sampling strategy

Four sampling campaigns were conducted in the months of March 2017, June 2017, November 2017, and May 2018. According to the rates of accumulated precipitation over 3 days (the precipitation rate reaching the ground over the period of 3 days before sampling), the samplings in March 2017 and May 2018 occurred under low accumulated precipitation (< 5 mm), whereas the sampling in June 2017 and November 2017 occurred under higher accumulated precipitation (> 5 mm). In each sampling campaign, five stations were sampled on the rivers that compose the drainage basin of the lagoon complex, and five stations were sampled in the lagoons of Tijuca and Marapendi (Fig. 1). The sampling stations in the rivers were accessed by car. The sampling stations in the lagoons were accessed using a small boat. The depths of the sampling stations were always lower than 2.5 m. A 3-liter Niskin bottle was used to collect water samples in subsurface (~0.5 m depth). The samples were conditioned (fixed and/or maintained in ice in the dark) for further analysis in the laboratory. A calibrated multiparametric Sonde (YSI, Professional Plus Model) measured in situ the salinity, temperature, and levels of dissolved oxygen (DO). The DO probe (optical optode) was calibrated every day the instrument was used through a 1-point calibration in water-saturated air. The accuracy was estimated at about ± 0.2 mg L^{-1} or 2% of reading. The samplings were always conducted during the ebb tide, to assess the major contribution from land runoff. It is important to point that we were not allowed to access the lagoons of Camorim and Jacarepagua due to the presence of an "ecological barrier," which prevented the boat navigation inside these water bodies (Fig. 1).

Laboratory analysis

Whatman GF/F filters were used for chlorophyll *a* (Chl *a*) analysis and the filtrate for nutrients and TA analysis. All the filters were pre-combusted (at 500°C for 6 h). Chl *a* concentrations were extracted in 90% acetone and quantified spectrophotometrically before and after acidification of the samples, with formulations and corrections proposed by Lorenzen (1967). Dissolved inorganic nitrogen, including ammonium (NH_4^+), nitrite (NO_2^-), and nitrate (NO_3^-), was quantified by the colorimetric method as in Grasshoff et al. (1999). TA was determined on 60 mL of filtrate using the Gran (1952) electro-titration method with an automated titration system (Mettler Toledo model T50). The reproducibility of TA was about 3 μmol kg^{-1} (n = 7). Measurements were compared to certified reference material (CRM, provided by A. G. Dickson from Scripps Institution of Oceanography) and consistent at a maximum accuracy level of 5 μmol kg^{-1}. pH was measured with a WTW 3310 pH meter equipped with a SenTix 41 electrode, calibrated in the National Institute of Standards and Technology (NIST) scale, using a three-point standard (pH 4.01, pH 7.00, and pH 10.01), always before and after each sampling campaign. The precision of the pH measurements was about 0.01 (after seven verifications against standards).

Samples for dissolved CH_4 were collected in 30 ml of preweighted serum glass bottles and completely filled with water using a homemade sampler that prevents gas exchanges and bubble formation. After sealing, 0.2 ml of saturated mercuric chloride was added in all bottles to prevent microbial activities. In the laboratory, a headspace of 10 mL of N_2 was created in the samples, followed by a vigorous agitation to obtain a complete equilibrium between the air and water phases inside the bottles (Abril et al. 2007). CH_4 concentrations were determined by gas chromatography (GC) (Shimadzu GC-2014 – Greenhouse) equipped with a 1 mL injection loop, a packed Porapak Q column, an ultrapure N_2 (99.999 %) as carrier gas, and a flame ionization detector (FID). The column oven and FID temperatures were set at 80°C and 250°C, respectively. Certified CH_4 standards (1517, 4987, and 10,096 ppm; White

Martins Certified Material, RJ, Brazil) were used for calibration. In situ CH_4 concentrations were calculated, taking into account the volume of water and headspace in the vial and solubility coefficient of methane of Yamamoto et al. (1976) as functions of temperature and salinity. Reproducibility of the CH_4 analysis was better than 5%.

Calculations

Carbonate system

The pCO_2 values and DIC concentrations were calculated using the concentrations of TA, pH, nutrients, seawater temperature, and salinity by the CO2calc 1.2.9 program (Robbins et al. 2010). The dissociation constants for carbonic acid were those proposed by Mehrbach et al. (1973) refitted by Dickson and Millero (1987), the borate acidity constant from Lee et al. (2010), the dissociation constant for the HSO_4^- ion from Dickson (1990), and the CO_2 solubility coefficient of Weiss (1974). For the anoxic/hypoxic waters, we calculated the pCO_2 and DIC using the update version of the program CO2SYS that includes acid-base system of NH_4^+ to TA (Xu et al. 2017).

The excess of DIC and apparent utilization of oxygen

The excess of DIC (E-DIC, μmol kg^{-1}) was calculated according to Abril et al. (2003):

$$\mathrm{E{-}DIC} = \mathrm{DIC_{sample}} - - \mathrm{DIC_{equilibrium}},$$

where DIC_{sample} represents the measured concentration of DIC (μmol kg^{-1}) and $DIC_{equilibrium}$ is the theoretical DIC at atmospheric equilibrium (μmol kg^{-1}). $DIC_{equilibrium}$ was calculated from observed TA and the atmospheric pCO_2 measured in the estuary.

The apparent oxygen utilization (AOU, μmol kg^{-1}) was calculated as proposed by Benson and Krause (1984):

$$\mathrm{AOU} = \mathrm{DO_{equilibrium}}{-}\mathrm{DO_{sample}}$$

where DO_{sample} is the measured DO and $DO_{equilibrium}$ is the DO saturation.

End-member mixing models

We applied mixing models to investigate the gains and losses of TA and DIC along the estuary. The model assumes conservative mixing for a solute (E) according to Samanta et al. (2015):

$$E_{\mathrm{mix}} = E_{\mathrm{freshwater}} F_{\mathrm{freshwater}} + E_{\mathrm{marine}}(1{-}F_{\mathrm{freshwater}})$$

where E_{mix} is the concentration of a given solute during conservative mixing (in our case TA and DIC), and the subscripts freshwater and marine indicate the end-member concentrations in the river and the ocean, respectively. The freshwater fraction ($F_{freshwater}$) is calculated as:

$$F_{\mathrm{freshwater}} = 1{-}\mathrm{Sal_{sample}}/\mathrm{Sal_{marine}}$$

where Sal is the salinity and the subscript sample refers to the in situ values for each station. As we did not perform the sampling in the marine end-member, we take the values of marine end-member from a published study, which investigated the carbonate chemistry during an annual cycle in an adjacent coastal embayment including the offshore waters (Cotovicz et al. 2015).

Calculations of air-water GHG fluxes

Diffusive fluxes of CO_2 and CH_4 at the air-water interface were computed according to the following equation:

$$\mathrm{F(GHG)} = \mathrm{k}\ (\Delta\mathrm{GHG})$$

where F(GHG) represents the diffusive fluxes of CO_2 and CH_4, k represents the gas transfer velocity of a given gas at a given temperature, and ΔGHG represents the concentration gradient between the water and the water at equilibrium with the overlying atmosphere. The considered atmospheric partial pressures of CO_2 and CH_4 were considered, respectively, 410 ppmv and 1.80 ppmv, which correspond to global averages of atmospheric GHG concentrations. These values are consistent with previous direct measurements of CO_2 and CH_4 atmospheric concentrations realized near to the study area (Cotovicz et al. 2015, 2016).

To calculate the gas transfer velocity, we first normalized a Schmidt number, applying the following equation (Jähne et al. 1987):

$$\mathrm{k} = k_{600}\left(600/\mathrm{Sc_{g,T}}\right)^{\mathrm{n}}$$

where k_{600} is the gas transfer velocity normalized to a Schmidt number of 600 (Sc = 600, for CO_2 at a temperature of 20°C), $Sc_{g,T}$ is the Schmidt number of a gas at a giver temperature (Wanninkhof 1992), and n is related to wind velocity, being equal to 2/3 for wind speed < 3.7 m s^{-1} and equal to 1/2 for higher wind velocities (Jähne et al. 1987; Guérin et al. 2007).

We used three empirical equations to derive k_{600} values: the parameterization as a function of wind speed applied for oceanic waters by Wanninkhof (1992, W92), the parameterization as a function of wind speed estimated for estuarine ecosystems by Raymond and Cole (2001, RC01), and the parameterization as a function of wind speed produced by regressing the literature data in coastal environments by Jiang et al. (2008; J08). The three parameterizations cover an important variability of values, with the value of W92 providing the lowest estimations and that of J08 providing the highest values of k_{600}.

The W92, RC01, and J08 parameterizations can be calculated applying the following equations:

$$k_{600}(\mathrm{W92}) = 0.31(\mathrm{U}_{10})^2$$
$$k_{600}(\mathrm{RC01}) = 1.91\mathrm{e}^{0.35\mathrm{U}10}$$
$$k_{600}(\mathrm{J08}) = 0.314(\mathrm{U}_{10})^2 - 0.436\mathrm{U}_{10} + 3.99$$

where k_{600} is the gas transfer velocity normalized to a Schmidt number of 600 (cm h^{-1}) and U_{10} is the wind speed at 10-m height (m s^{-1}). Water-to-air CO_2 fluxes were calculated using the GHG concentrations for each sampled station. After, these fluxes per station were daily averaged considering the "polluted rivers" stations (1 to 5) and the "lagoons" stations (5 to 10) using the averaged gas transfer velocities calculated for each day of sampling. Gas transfer velocities were calculated from wind speed data, which were logged every hour and averaged at 12-h intervals throughout the sampling days. The fluxes calculated for each domain, i.e., "polluted rivers" and "lagoons," were separated in nighttime (measurements conducted before 09:30 a.m.) and daytime (measurements conducted after 09:30 a.m.) periods to account for the diel wind patterns and then integrated over the entire sampled period and the entire sampled area. We divided the gas transfer velocities in these periods because the region receives important influences from marine brises, where the winds are stronger during midday/afternoon than during the night/early morning (Amarante et al. 2002; Cotovicz et al. 2015). The meteorological data were kindly provided by the National Institute of Meteorology (INMET). To compare the air-water fluxes of CH_4 with those of CO_2, we used the concepts of global warning potential (GWP) and CO_2 equivalent emissions (CO_2-eq), by considering that 1 g of CH_4 has a GWP equivalent to 28 g of CO_2 on a time horizon of 100 years (IPCC 2013).

Statistical analysis

To verify if the data followed parametric or non-parametric distributions, we applied the Shapiro-Wilk test. As the dataset was not normally distributed, we used the non-parametric and non-paired Mann-Whitney test to compare the average differences between the river and lagoon stations for each sampling camping (spatial variability). The non-parametric and paired Friedman test was applied to compare the averages of sampled stations considering the different sampling campaigns (temporal variability). Linear and non-linear regressions were calculated to compare the distributions and correlations between variables. All statistical analysis were based on $\alpha = 0.05$. We used the GraphPad Prism 6 program (GraphPad Software, Inc., La Jolla, California) to perform the statistical tests.

Results

Ancillary parameters

The main parameters analyzed in this study are provided in Table 1, with averages, standard deviations, and ranges. The data were separated by sampling campaigns and by sampled stations (rivers and lagoon). Box plots of the main parameters, separated by sampling stations, with maximum, minimum, and medians are presented in the supplemental file (Online Resource Fig. S1). Water temperature was related to the period of the year. The highest temperatures were measured in summer, reaching a maximum of 29.0°C in March 2017, whereas the lowest temperatures were measured in winter/autumn, with a minimum of 20.4°C in November 2017. The water temperature did not present significant spatial differences when comparing rivers and lagoon (Mann-Whitney test, $p > 0.05$), except in the campaign of November 2017, when the lagoon stations presented lower temperature than the freshwaters (Mann-Whitney test, $p < 0.01$). The salinity at river stations was always closest to 0, except at stations 4 and 5, which present occasional saline intrusion reaching a maximum value of 5 (Table 1, Fig. 2). The salinity in the lagoon stations ranged between 6.6 and 34. As expected, the highest salinities were observed in the stations located closest to the mouth of the lagoon complex (stations 6 and 8).

DO concentrations exhibited strong depletion in the river stations, reaching values very close to 0 in almost all stations and sampling campaigns (Table 1; Fig. 2f). Exceptions were verified in station 4, which exhibited occasional occurrence of high DO concentrations. In the lagoons, the concentrations of DO were variable, usually exhibiting undersaturated conditions, with very little occasions of oversaturation with respect to the atmosphere equilibrium (Fig. 2f). This pattern of DO distributions was inverse of that verified for the concentrations of NH_4^+ (Fig. 2g). The highest values of NH_4^+ were found in the hypoxic/anoxic freshwaters, reaching an extreme maximum concentration of 5660 μmol L^{-1}. The concentrations of NH_4^+ decreased exponentially with the increase of salinity and with the increase of DO concentrations (Fig. 3a), reaching a minimum of 3.5 μmol L^{-1}. As expected, DO distributions were positively related to the concentrations of NO_3^- (Fig. 3b). NO_3^- exhibited low concentrations in the polluted rivers, with increasing tendency with the increase of salinity and DO concentrations (Fig. 3b). The concentrations of Chl *a* were significantly lower in the freshwaters compared to the lagoon stations (Mann-Whitney test, $p < 0.01$) (Fig. 2h). In general, the anoxic/hypoxic freshwaters presented low concentrations of Chl *a*, except at station 4, which presented occasional occurrence of high Chl *a* concentrations, with an extreme highest value of 347 μg L^{-1}, and coincident with a peak in DO

Table 1 Mean, standard deviation, minimum, and maximum values of the main water properties of JLC investigated in this study, separated in "river" and "lagoon" stations, for all sampling campaigns

	Temp. (°C)	Salinity	pH (NBS)	Chl *a* (μg L^{-1})	DO (%sat)	TA (μmol kg^{-1})	DIC (μmol kg^{-1})	pCO_2 (ppmv)	CH_4 (nmol L^{-1})	$N\text{-}NH_4^+$ (μmol L^{-1})
March 2017										
Rivers	26.6 ± 1.1	1.0 ± 1.1	7.09 ± 0.07	7.1 ± 12.9	2.1 ± 1.7	3004 ± 194	3435 ± 306	13,641 ± 3211	47,285 ± 22,731	2154 ± 990
	23.9/27.7	0.2/4.0	7.02/7.26	0.2/30.2	0.1/6.1	2618/3313	3012/3846	8931/16,974	25,573/70,913	887/3333
Lagoons	27.5 ± 1.1	19.3 ± 3.6	7.90 ± 0.05	13.9 ± 9.9	57.4 ± 23.9	1868 ± 338	1802 ± 401	872 ± 240	392 ± 304	312 ± 249
	25.9/29.0	11.2/24.9	7.84/7.97	5.3/30.4	24.3/86.2	1431/2263	1385/2233	577/1226	92/723	129/677
June 2017										
Rivers	22.5 ± 0.3	0.2 ± 0.0	7.12 ± 0.08	0.6 ± 0.2	3.9 ± 0.8	1400 ± 836	1663 ± 1408	6878 ± 7801	43,637 ± 17,408	2542 ± 432
	22.2/23.4	0.2/0.3	6.93/7.22	0.3/0.9	(2.0 5.5	572/3268	652/4028	1927/20,417	30,677/68,336	1028/3477
Lagoons	22.9 ± 1.0	16.1 ± 5.2	8.10 ± 0.43	17.0 ± 7.1	81.8 ± 38.9	1694 ± 229	1599 ± 358	821 ± 708	1415 ± 1878	104 ± 45
	22.0/24.6	6.6/24.8	7.63/8.67	9.58/26.71	35.0/140.0	1497/2047	1267/2032	109/1603	47/4660	58/177
November 2017										
Rivers	25.6 ± 0.6	1.2 ± 1.5	7.51 ± 0.45	73.3 ± 153.5	28.2 ± 42.7	2949 ± 466	3029 ± 755	8127 ± 5066	159,178 ± 105,131	3353 ± 1721
	24.9/26.7	0.2/5.1	7.13/8.64	2.1/347.9	1.0/135.0	2450/3680	2003/3918	218/13,742	550/288,572	868/5660
Lagoons	21.6 ± 1.3	26.9 4.9	8.12 ± 0.09	34.6 ± 35.4	87.4 ± 12.2	2169 ± 495	1975 ± 515	523 ± 217	1121 ± 1610	35 ± 47
	20.4/24.2	21.2/31.8	8.04/8.30	3.6/77.0	73.1/112.0	1449/2567	1205/2287	215/725	199/3528	3.5/105
May 2018										
Rivers	25.9 ± 0.4	0.6 ± 0.4	7.18 ± 0.22	-	1.7 ± 0.4	2860 ± 265	3226 ± 259	11,500 ± 5398	-	3126 ± 1348
	25.3/26.6	0.2/1.6	6.97/7.63		1.4/2.8	2399/3062	2853/3560	3856/17,096		768/4078
Lagoons	24.9 ± 1.0	26.0 ± 5.6	7.92 ± 0.04	24.0 ± 5.9	71.0 ± 9.4	2173 ± 326	2055 ± 292	843 ± 117	-	294 ± 332
	23.7/27.2	16.0/34.0	7.84/7.97	18.3/32.7	52.4/85.6	1659/2441	1594/2319	716/981		96/876

concentration (Fig. 2f,h). In the lagoon stations, the distributions of Chl *a* were highly variable ("patch distributions"), exhibiting the highest concentrations at intermediate salinities (10–20). The results of Chl *a* for the sampling in May 2018 are not presented due to problems during sampling.

Carbonate chemistry

The distributions of TA and DIC were very different considering the river and lagoon stations (Fig. 2a,b). TA and DIC concentrations were significantly higher in freshwaters compared to the lagoon waters (Mann-Whitney test, $p < 0.001$), except in the campaign in June 2017, when the river TA and DIC concentrations were lower than the lagoons (Fig 2a,b). The ranges of concentrations of freshwater TA were between 572 and 3680 μmol kg^{-1}, and for DIC, these ranges varied between 652 and 4026 μmol kg^{-1}. Considering the lagoon stations, these ranges varied between 1431 and 2567 μmol kg^{-1} for TA and between 1205 and 2319 μmol kg^{-1} for DIC. DIC and TA distributions did not exhibit a clear pattern with salinity. In the campaign in November 2017, the tendency between TA and DIC versus salinity was positive, whereas for the other three sampling campaigns, this relationship was negative. However, in all sampling campaigns, the distributions of TA and DIC showed large deviations from the conservative mixing considering the end-member mixing models (Fig. 4). In general, the lagoon stations presented negative values of ΔTA and ΔDIC (Δ representing the differences between measured DIC and/or TA concentrations and the expected value for the conservative mixing), indicating important consumption of DIC and TA in the mixing regions. The highest values of TA were found in hypoxic/anoxic waters, presenting positive relationship with NH_4^+ concentrations and negative relationship with NO_3^- (Fig. 3c,d). A TA minimum was observed in the middle salinity region, corresponding to lowest NH_4^+, highest NO_3^-, DO, and Chl *a* concentrations.

As expected, the river waters presented low values of pH, with a minimum value of 6.93 and average of 7.22 ± 0.20 (Table 1; Fig. 2d). The pH increased inside the lagoons, presenting the highest concentrations in the intermediate salinities (10–20), and coincident with the highest values of Chl *a*, despite the absent significant correlation between these parameters. The values of pH were strongly correlated to the distributions of DO concentrations (Fig. 5a).

Dissolved GHG concentrations and air-water fluxes

As shown for the most parameters analyzed in this study, the averaged values of pCO_2 were highly different considering the "polluted rivers" and "lagoons" for all the sampling campaigns (Table 1, Fig. 2c). High supersaturated conditions were observed in the anoxic/hypoxic river waters. The highest pCO_2 value was 20,417 ppmv. Freshwater pCO_2 exceeding 12,000 ppmv was verified in all sampling campaigns. In the

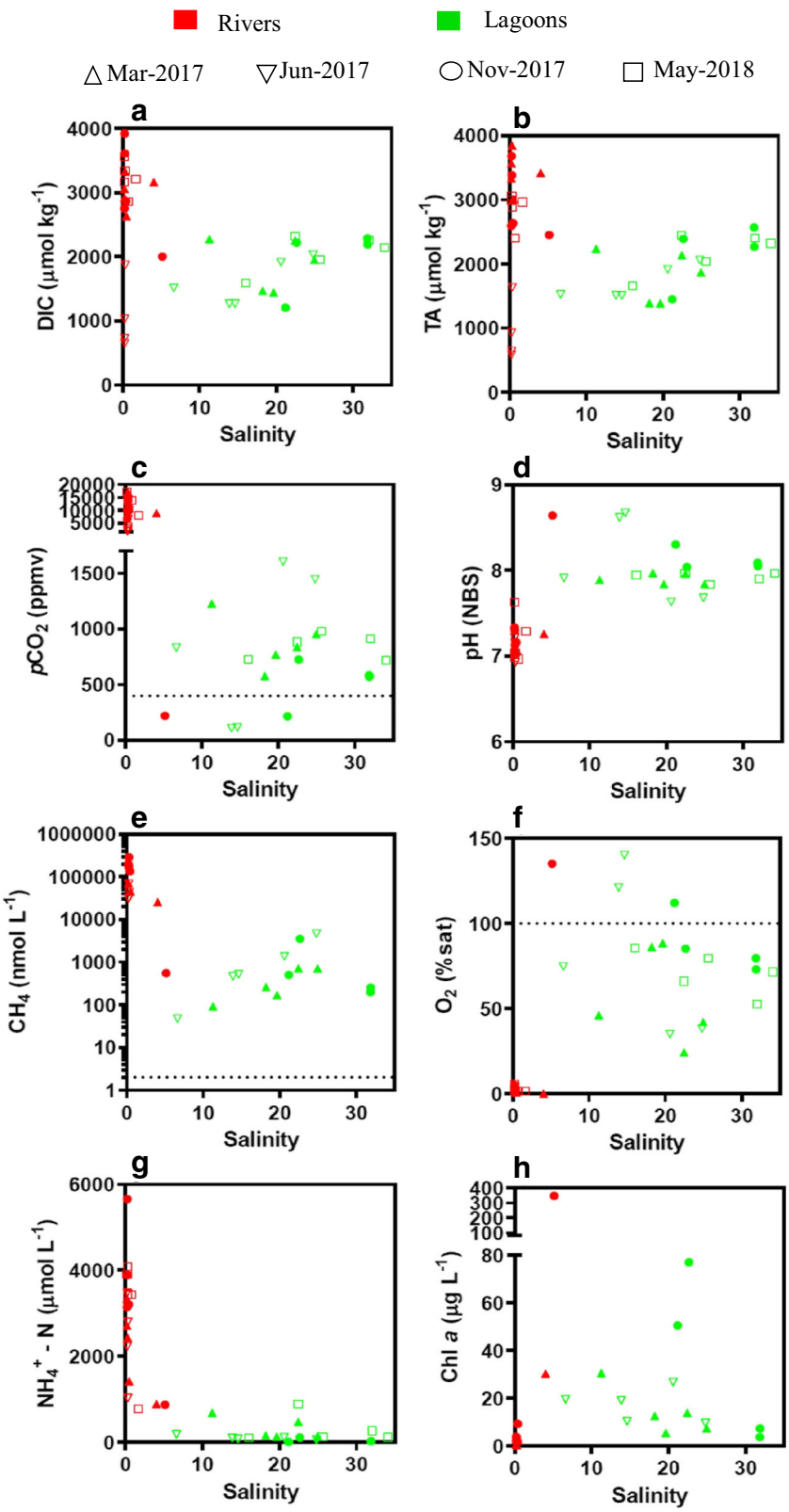

Fig. 2 Distributions of the main parameters analyzed in this study along the salinity gradient. The red circles represent the river stations, whereas the green circles represent the lagoon stations

lagoons, the values decreased substantially, lowering about one order of magnitude. The average value was 764 ± 320 ppmv in the lagoon stations. Values of pCO_2 below the equilibrium with the atmosphere were verified only in four occasions, being three in the lagoons and one in the river domain, all related to high concentrations of Chl *a* and

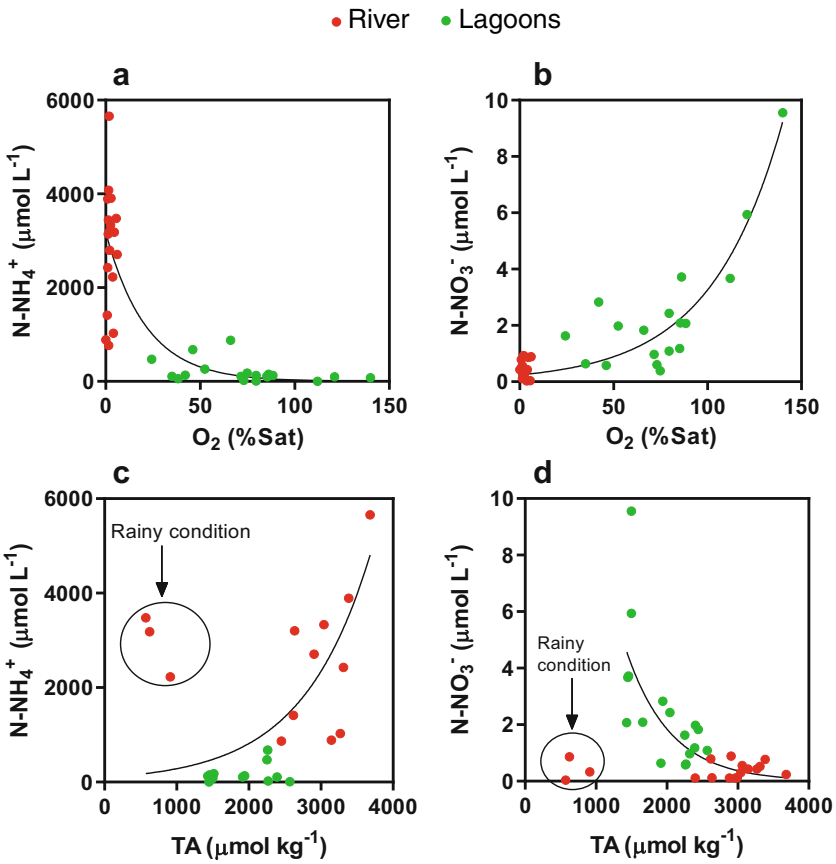

Fig. 3 Scatterplots between **a** NH_4^+ and O_2, **b** NO_3^- and O_2, **c** NH_4^+ and TA, and **d** NO_3^- and TA including all stations and sampling campaigns

oversaturation of DO (Fig. 2c,d,f). Considering all data (river and lagoon stations), the averaged values of pCO_2 were significantly different considering the sampling campaigns ($p <$ 0.05; Friedman test). We used the relationship between the AOU and E-DIC to investigate the influence of biological processes on the concentrations of DIC and DO (Fig. 5b). The scatterplot of E-DIC versus AOU shows that the data of the lagoon stations were close to the 1:1 line. This line represents the theoretical quotient of photosynthesis and respiration. The river stations presented a marked deviation above the 1:1 line, corresponding to hypoxic/anoxic conditions.

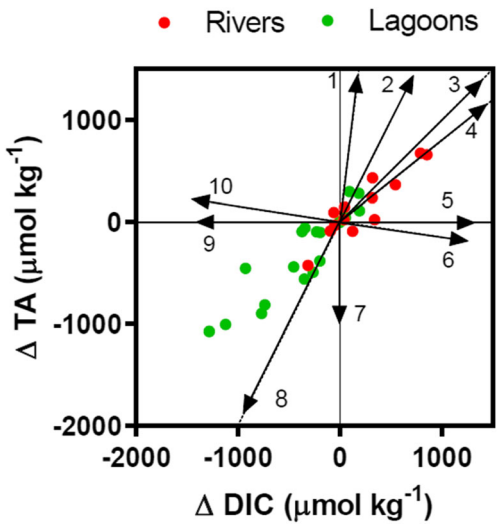

Fig. 4 Deviations from conservative mixing lines of TA (ΔTA) as a function of DIC (ΔDIC) in the river stations (red dots) and lagoon stations (green dots), for all sampling campaigns. The unitless directional vectors representing the slopes of the following processes: (1) iron reduction; (2) carbonate dissolution; (3) sulfate reduction; (4) denitrification; (5) CO_2 influx (ingassing); (6) aerobic respiration; (7) sulfur oxidation, iron oxidation, and nitrification; (8) carbonate precipitation, (9) CO_2 efflux (degassing); and (9) primary production

For the distributions of dissolved CH_4 concentrations, the behavior was similar to that of pCO_2, exhibiting extreme supersaturation conditions in the hypoxic/anoxic river waters (Figs. 2e and 5c). The highest CH_4 concentration was 288,572 nmol L^{-1}, coincident with anoxic conditions (0.1 $\%O_2$), representing one of the uppermost concentrations ever reported in coastal waters worldwide. All the concentrations of dissolved CH_4 were higher than 25,000 nmol L^{-1} in the polluted rivers, except in one situation in station 4 (November 2017), which displayed concentration of 550 nmol L^{-1}, and coincident with the high concentration of Chl *a* and supersaturation of DO. In the lagoons, the CH_4 concentrations decreased exponentially compared to the rivers, spanning between two to three orders of magnitude. CH_4 concentrations in the lagoons ranged between 47 and 4666 nmol L^{-1}. The CH_4 concentrations were significantly different considering the sampling campaigns, including all data, and the river and lagoons stations separately (rivers x lagoons). The highest

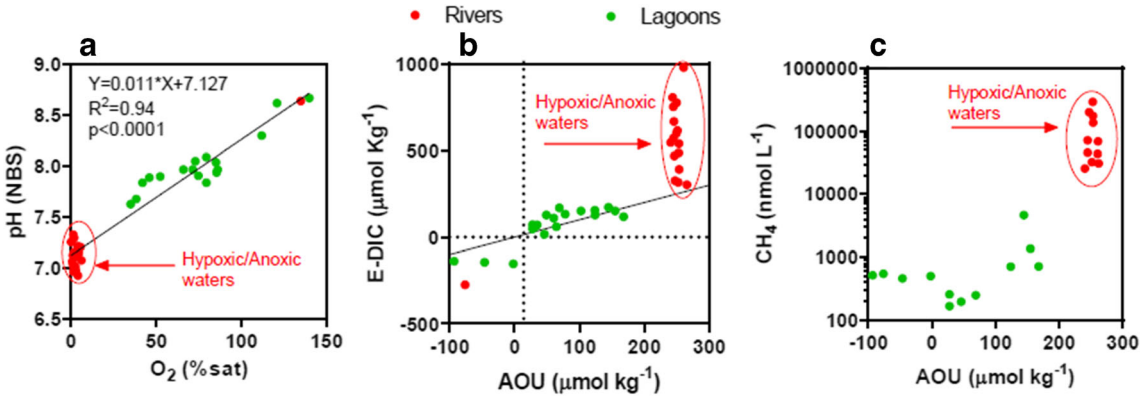

Fig. 5 Graph a) shows the relationship between pH and O_2, for all sampling campaigns. The black line represents the linear regressions. Graph b) shows the relationship between the excess dissolved inorganic carbon (E-DIC) and apparent utilization of oxygen (AOU). The 1:1 black line represents the quotient between CO_2 and O_2 during the processes of photosynthesis and respiration. The green line represents the linear regressions considering only the lagoon stations. Graph c) shows the relationship between the concentrations of CH_4 and AOU. Note that the *y*-axis is logarithmic. Red dots are the station in the rivers, and green dots are the stations in the lagoons

concentrations of CH_4 in the river were observed in November 2017, which was the sampling with the lower rates of accumulated precipitation. The results of CH_4 in the month of May2018 are not presented due to logistical problems during sampling.

The relationship between dissolved CH_4 concentrations and pCO_2 values was positive and statistically significant for all sampling campaigns (Fig. 6). However, it is clear that the tendency was different considering the sampled periods, with distinct slopes and intercepts. In two samplings (March 2017 and November 2017), the relationship showed a linear tendency between these two parameters shown. In the sampling of June 2017, the relationship followed a non-linear trend, fitting in an exponential growth equation type "one phase decay." This figure also showed that for similar values of pCO_2 (~15,000 ppmv), the concentrations of CH_4 can span one order of magnitude (from ~25,500 to 170,000 nmol L^{-1}).

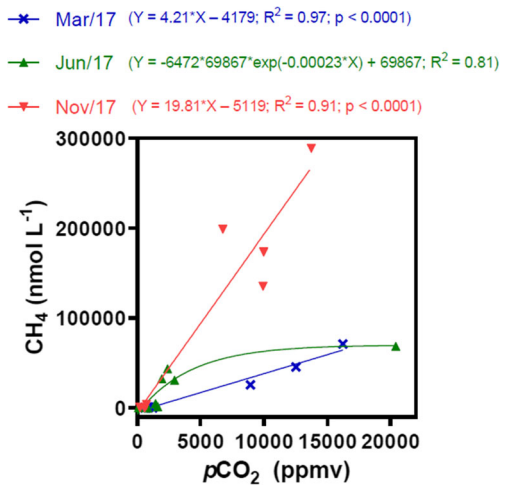

Fig. 6 CH_4 dissolved concentrations vs. average partial pressure of CO_2 (pCO_2) for the sampling campaigns in March 2017, June 2017, and November 2017. For March 2017, the blue line represents the linear regressions. For March 2017 and November 2017, the relationship showed a linear tendency, whereas for June 2017, the relationship followed a non-linear trend, fitting in an exponential growth equation

The values of gas transfer velocities as well as fluxes of CH_4 and CO_2 are presented in Table 2. The gas transfer velocities were lower using the parametrization of W92, followed by the parameterization of RC01 and J08. The k_{600} values ranged between 0.99 and 5.10 m s^{-1} for the river-sampled stations, whereas for the lagoon stations, this range was between 1.12 and 6.13 m s^{-1}. In general, k_{600} did not present significant differences considering the sampling campaigns ($p > 0.05$; Friedman test), except in the sampling of November 2017 in the second day of sampling, when the values of wind speed were higher. The calculated diffusive fluxes of CO_2 and CH_4 at the air-water interface showed marked differences considering the river and lagoon stations, with the river showing very higher emissions than the lagoons (Table 2). The fluxes were calculated for each sampling campaign, including fluxes for the river and lagoon stations separately, as well as the fluxes with all data (area-weighted). The emissions of CO_2 and CH_4, with the averages and standard deviations calculated with the three parameterizations, are presented in supplemental file (Online Resource Fig. S2). The river stations always showed high emissions of CO_2, with averages of emissions ranging between 72.85 and 652.48 mmol C $m^{-2}d^{-1}$. For the lagoons, the emissions spanned between one to two orders of magnitude lower than the rivers. The emissions in the lagoons ranged between 4.27 and 17.59 mmol C m^{-2} d^{-1}. The samplings in March 2017 and May 2018 showed the higher emissions, whereas the samplings in June 2017 and November 2017 showed the lower emissions. Considering all the lagoon complex (area-weighted including rivers and lagoons stations), the CO_2 emissions ranged between 9.8 and 70.5 mmol C m^{-2} d^{-1}. For the diffusive emissions of CH_4, the rivers showed extreme high values of degassing, with the magnitudes of emissions being between two and three orders of magnitude higher than those verified in the lagoon stations.

Table 2 Average values of gas exchange velocity (k_{600}) and air-water CO_2 and CH_4 fluxes calculated according to Wanninkhof (1992) (W92), Raymond and Cole (2001) (RC01), and Jiang et al. (2008) (J08), separated by river and lagoon stations and integrated for entire superficial area, for each sampling campaign

	k_{600} (cm h^{-1})			CO_2 flux (mmol m^{-2} d^{-1})			CH_4 flux (mmol m^{-2} d^{-1})		
	W92	RC01	J08	W92	RC01	J08	W92	RC01	J08
March 2017									
Rivers (1.07 km^2)	2.84	4.88	5.10	363.34	624.33	652.48	38.19	65.63	68.59
Lagoons (12.08 km^2)	2.24	4.40	4.75	8.95	17.59	18.99	0.24	0.48	0.51
All system area-weighted (13.15 km^2)				37.78	66.95	70.50	3.33	5.78	6.05
June 2017									
Rivers (1.07 km^2)	2.06	4.24	4.64	126.25	259.86	284.38	22.58	46.47	50.85
Lagoons (12.08 km^2)	1.12	3.44	4.15	4.46	13.70	16.53	0.38	1.18	1.42
All system area-weighted (13.15 km^2)				14.36	33.72	38.32	2.19	4.86	5.45
November 2017									
Rivers (1.07 km^2)	0.99	3.32	4.09	72.85	244.32	300.98	44.80	150.27	185.12
Lagoons (12.08 km^2)	4.50	6.24	6.13	4.27	5.93	5.82	1.12	1.56	1.53
All system area-weighted (13.15 km^2)				9.85	25.32	29.83	4.68	13.66	16.47
May 2018									
Rivers (1.07 km^2)	2.24	4.24	4.75	237.85	450.21	504.37			
Lagoons (12.08 km^2)	2.06	4.40	4.64	7.25	15.49	16.33			
All system area-weighted (13.15 km^2)				26.01	50.86	56.04			

The ranges of riverine CH_4 emissions were between 22.58 and 185.12 mmol C m^{-2} d^{-1}. In lagoons, the emissions ranged between 0.2 and 1.4 mmol C m^{-2} d^{-1}. Considering all the lagoon complex (area-weighted of rivers and lagoons), the CH_4 emissions ranged between 2.2 and 16.5 mmol C m^{-2} d^{-1}.

Discussion

High concentrations of TA and DIC in hypoxic/anoxic river waters

TA is generally considered as a relative conservative property of natural waters (Kempe 1990; Wolf-Gladrow et al. 2007). In estuaries, TA generally shows a linear distribution versus the salinity following conservative mixing. However, in coastal regions enriched in organic matter where anaerobic processes are significant, the assumption of conservativity of TA can be abusive because the reactions of reduction and oxidation are coupled to proton production and consumption, contributing to changes in TA (Abril and Frankignoulle 2001; Hu and Cai 2011). Indeed, anaerobic decomposition of organic matter by denitrification, reduction of iron and manganese oxides, and sulfate reduction are proton-consuming processes that will produce TA and DIC with specific stoichiometric ratios. Table 3 presents the stoichiometry of main chemical reactions involved in generation/consumption of TA in coastal regions. In the polluted rivers of the JLC, it is clear that the permanent hypoxic/anoxic conditions favor the production of TA and DIC in waters and sediments due to the high TA concentrations in the freshwater end-members in almost all sampling campaigns. The exception was verified in the sampling of

Table 3 Stoichiometry of main diagenetic reactions that significantly affect TA in the environment. The reactions were separated in positive TA alterations (most common in anaerobic environments) and negative TA alterations (most common in aerobic environments)

			Net change	
	Positive TA alterations	Chemical reaction	DIC	TA
1	Ammonification	$R\text{-}NH_2H + H_2O + H^+ \rightarrow R\text{-}OH + NH_4^+$	0	+2
2	Denitrification	$CH_2O + 0.8NO_3^- + 0.8H^+ \rightarrow CO_2 + 0.4N_2 + 1.4H_2O$	+1	+0.8
3	Iron reduction	$CH_2O + 2Fe_2O_3 + 8H^+ \rightarrow CO_2 + 5H_2O + 4Fe^{2+}$	+1	+8
4	Sulfate reduction	$2CH_2O + SO_4^{2-} + 2H^+ \rightarrow 2CO_2 + 2H_2O + H_2S$	+2	+2
5	Manganese reduction	$CH_2O + 2MnO_2 + 3H^+ \rightarrow HCO_3^- + 2Mn^{2+} + 2H_2O$	+1	+4
6	$CaCO_3$ dissolution*	$CaCO_3 \rightarrow CO_3^{2-} + Ca^{2+}$	+1	+2
			Net change	
	Negative TA alterations	Chemical reaction	DIC	TA
7	Nitrification	$NH_4^+ + 2O_2 \rightarrow NO_3^- + 2H^+ + H_2O$	0	−2
8	Iron oxidation	$Fe^{2+} + O_2 + 10H_2O \rightarrow 4Fe(OH)_3 + 8H^+$	0	−8
9	Sulfide oxidation	$1/2HS^- + O_2 \rightarrow 1/2SO_4^{2-} + 1/2H^+$	0	−1
10	Manganese oxidation	$2Mn^{2+} + O_2 + 4HCO_3^- \rightarrow 2MnO_2 + 4CO_2 + 2H_2O$	0	−4
11	$CaCO_3$ precipitation*	$Ca^{2+} + CO_3^{2-} \rightarrow CaCO_3$	−1	−2

* Exceptions are the reactions of precipitation and dissolution of $CaCO_3$, which are not necessarily linked to aerobic/anaerobic conditions

June 2017 that occurred under conditions of high accumulated precipitation when 3 river stations presented low TA, suggesting dilution during rainy conditions. The rivers of the JLC watershed are inserted in a region of low-carbonate minerals, which generates very low concentrations of TA in freshwaters (Meybeck and Ragu 2012). The background values of TA in the regions located upstream to the urban influences are low (~ 300–400 μmol kg^{-1}). Considering that freshwater TA concentrations ranged between 572 and 4022 μmol kg^{-1}, the contribution of anaerobic processes on the generation of TA is estimated at about 30 to 90%. These values are very similar to those found in the highly polluted Scheldt estuarine basin in the Belgium (Abril and Frankignoulle 2001), where the authors found bicarbonate (HCO_3^-) concentrations 2–10 times higher than the representative concentrations reported in pristine basins. In addition, 22 to 63% of TA concentrations were attributed to process involving nitrogen cycling (ammonification, nitrification, and denitrification) in the low-salinity region of the Scheldt Estuary.

The plot between the deviation from the conservative mixing of TA and DIC (ΔTA and ΔDIC) reveals regions of gains and losses of TA and DIC along the lagoon complex (Fig. 4). Data points from the river stations presented always positive values, consistent with the production of TA and DIC. The distributions of ΔTA and ΔDIC in the polluted rivers (red points) follow mainly the vectors that represent the processes of carbonate dissolution, sulfate reduction, and denitrification (see the figure caption for detailed descriptions and Table 3). Carbonate dissolution is unlikely to occur due to the low carbonate concentrations in the rivers of this region (Meybeck and Ragu 2012), whereas denitrification and sulfate reduction are likely to occur in a significant way. Overall, the highest concentrations of TA were coincident with the highest concentrations of NH_4^+ (Fig. 3c), possibly reflecting the denitrification process. The exception was verified in June 2017, which occurred under high rainy conditions (highest accumulated precipitation before 3 days of sampling), when TA seemed to be diluted and NH_4^+ concentrations still high possibly reflecting the urban runoff. Overall, the rivers of the JLC presented remarkably high NH_4^+ concentrations, in the same order of magnitude verified only in the highly polluted Adyar Estuary – India (average between 1200 and 3000 μmol L^{-1}; Nirmal-Rajkumar et al. 2008) and well above than found in rivers enriched in nitrogen (McMahon and Dennehy 1999). These values are comparable to those found in municipal wastewaters (Hammer and Hammer 2012). Denitrification produces DIC and TA that generates nitrogen (N_2), which in turn escapes to the atmosphere (Abril and Frankignoulle 2001; Thomas et al. 2009). This represents an irreversible generation of TA, because the product resists or escapes re-oxidation by oxygen (Thomas et al. 2009). The same is valid for the sulfate reduction, which generates hydrogen sulfite (H_2S) (Thomas et al. 2009). However, TA, NH_4^+, NO_3^-, and DO concentrations in the intermediate salinities suggest that during river-ocean mixing, important processes of re-oxidation are occurring that can be a sink for TA compensating the TA generated in the anoxic waters (Hu and Cai 2011; Gustafsson et al. 2019) (see the next section of the manuscript).

The aerobic respiration can also contribute to the increases of DIC concentrations in heterotrophic waters (Borges and Abril 2011); however, in these polluted and anoxic riverine stations, this process seems to be minor compared to anaerobic/anoxic processes. This can be confirmed by looking at the relationship between E-DIC and AOU (Fig. 5b). The

data points of the river stations present strong deviation above the 1:1 line, which represents the theoretical quotient between photosynthesis and respiration. This means that additional processes are contributing to the production of DIC that is not linked to the aerobic microbial respiration. This graph shows that the production of DIC can continue even if the oxygen is depleted. These conditions were verified in high pCO_2 estuaries and attributed mainly to lateral inputs of dissolved CO_2 and anoxic production in waters and sediments (Cai et al. 1999; Abril and Iversen 2002; Borges and Abril 2011). In addition, the relationship between AOU and E-DIC can also be affected by the more rapid equilibration of O_2 compared to CO_2 (Borges and Abril 2011). Like this, the waters tend to re-oxygenate faster than they emit CO_2 to the atmosphere because the buffering effect of bicarbonate concentration affects the CO_2 concentrations, but not the O_2 concentrations.

Carbonate chemistry in the lagoon waters

Contrary to rivers, the lagoon stations present important losses of TA and DIC along the salinity gradient, with prevalence of negative values of ΔTA and ΔDIC in these more oxygenated waters (Fig. 4). Comparing the covariations of ΔTA and ΔDIC along the salinity gradient, the data points followed mainly the vectors representing the processes of sulfur oxidation, iron oxidation, and nitrification that are involved only in the consumption of TA, without the net effect on DIC (Abril and Frankignoulle 2001; Baldry et al. 2019; Rassmann et al. 2020). In the lagoons, the mixing of anoxic-acid freshwaters with well-oxygenated marine waters is associated with processes of re-oxidation of reduced by-products of organic matter degradation, generating titration of TA to dissolved CO_2 particularly evident in the middle salinity regions (Fig. 2). These intermediate saline waters (10–20) presented the lowest TA concentrations well below for both freshwater and marine end-members, coincident with minimum concentrations of NH_4^+ and maximum concentrations of NO_3^- and DO. The nitrification is a process that consumes TA, when NH_4^+ is oxidized to NO_3^-, producing $2H^+$ (Table 3; Frankignoulle et al. 1996; Abril and Frankignoulle 2001). TA concentrations present an important and inverse relationship with NO_3^- concentrations, corroborating this assumption (Fig. 3b). This suggests that this is an area where nitrification is complete, counteracting the process of denitrification that occurs in the anoxic freshwaters, compensating the TA generated in anoxic waters. In this way, the lagoon reflects a combination of processes, including denitrification and ammonification in anoxic conditions at low salinities and nitrification in well-oxygenated conditions at intermediate salinities. Indeed, the complete coupling of ammonification-nitrification-denitrification does not lead to net TA gain (Hu and Cai 2011). In addition, the re-oxidation of all other reduced compounds (H_2S, Fe^{2+}, Mn^{2+}, and also a part of CH_4) is probably also complete. However, it must be stressed that the re-oxidation of reduced species is often complex involving many intermediate steps and side products (Cai et al. 2017). In the JPL, the re-oxidation decreases TA concentrations down to 1500 μmol kg^{-1} (Fig 3), much lower than the end-member concentrations. Important re-oxidation processes were described in the high-polluted Scheldt basin, when the ecosystem changes from reducing to oxidizing conditions (Abril and Frankignoulle 2001).

Primary production is also apparently occurring in the mixing zone, generating significant uptake of DIC. Occasional occurrence of phytoplankton blooms was found in the lagoon stations (highest value of Chl *a* of 77 μg L^{-1} in November 2017), associated with a decrease in DIC concentrations and an increase of pH and dissolved oxygen (Fig. 5). In eutrophic systems like the JLC, planktonic primary production can be strongly stimulated by the high availability of nutrients in the water column, shallow depths, high temperature, and high incidence of photosynthetically active radiation (Cotovicz et al. 2015). The influence of biological activities on the carbonate chemistry is evidenced by comparing the E-DIC versus AOU values (Fig. 5b). Positive E-DIC and AOU values suggest that the system is predominantly heterotrophic. The regression line between E-DIC and AOU for the lagoon stations (green line) is very close to the line 1:1, suggesting that the processes of gross primary production and total respiration are coupled in the lagoons, but not in the rivers. This was also showed in the Guanabara Bay (Rio de Janeiro, Brazil), a eutrophic coastal embayment dominated by phytoplankton blooms (Cotovicz et al. 2015) and located close to the JLC. However, in the JLC, other biogeochemical processes described above like denitrification-nitrification and iron reduction-oxidation will also follow closely the 1:1 line (Table 3). The biological influences on the carbonate chemistry are also apparent in the relationship between O_2 and pH (Fig. 5a), which shows a strong significant and positive relationship ($R^2 = 0.94$, $p < 0.0001$). In general, the river stations present very low pH values coincident with hypoxic/anoxic conditions.

Spatial distributions of dissolved CO_2 and CH_4 in the JLC

Inner and low-salinity estuarine regions have been documented as heterotrophic and large CO_2 emitters (Frankignoulle et al. 1998). In several coastal waters worldwide, important CO_2 changes have been strongly related to eutrophication (Borges and Gypens 2010; Cai et al. 2011; Sunda and Cai 2012; Cotovicz et al. 2015; Brigham et al. 2019). Overall, when urban wastewater from megacities is discharged to estuarine waters, it enhances CO_2 outgassing, especially in turbid coastal waters (Frankignoulle et al. 1998; Zhai et al. 2007;

Sarma et al. 2012; Brigham et al. 2019). This property of high pCO_2 values is observed in the polluted rivers that compose the drainage basin of the JLC. The averaged values of pCO_2 in these rivers ranged between 6838 and 13,641 ppmv. Such high values were reported only in highly impacted estuaries, i.e., Tapti Estuary – India (Sarma et al. 2012), Scheldt Estuary – Belgium (Frankignoulle et al. 1998), and Pearl River – China (Guo et al. 2009). The river waters of the JLC presented an extreme oxygen depletion reaching anoxic conditions at the surface in almost all stations and sampling campaigns, all related to supersaturation of pCO_2. The wastewater contribution is corroborated by the very high NH_4^+ concentrations reaching concentrations measured in municipal wastewaters (Hammer and Hammer 2012).

Following the seaward direction, the levels of pCO_2 decrease exponentially with increasing salinity. This decrease is associated with degassing, biogeochemical processes, and mixing with low-pCO_2 marine waters (Borges and Abril 2011; Cotovicz et al. 2020). CO_2 degassing is strongest at the freshwater stations, taking into account that the dissolved concentrations are at the highest in this estuarine region, creating a steep gradient between the pCO_2 in the air and in the water. The freshwaters enters in the lagoon with highly reduced conditions, and the mixing with more oxygenated waters generates important processes of re-oxidation, as discussed above. The processes of nitrification and manganese, iron, and sulfide oxidation generate a production of protons that titrate TA to CO_2 in transitional oxic/anoxic estuarine regions (Abril and Frankignoulle 2001). In this way, the pCO_2 values reflect both the physical mixing and the biogeochemical processes. For intermediate to high salinities, the low values of pCO_2 values are expected due to the mixing with low-pCO_2 seawaters (Chen et al. 2013; Cotovicz et al. 2020), taking into account that the adjacent coastal waters present pCO_2 averaging 411 ppmv (Cotovicz et al. 2015). The uptake of CO_2 by primary producers is also occurring as revealed by the marked decline of pCO_2 within phytoplankton blooms at some stations. Overall, pCO_2 values did not present a clear seasonal trend; however, the lowest average of pCO_2 in the rivers was found in June 2017, when the accumulated precipitation was at highest levels, probably associated with dilution of river waters with rainwater.

Approaching the behavior generally found for CO_2, CH_4 concentrations are often much greater in the uppermost portion of estuaries (Upstill-Goddard et al. 2000; Middelburg et al. 2002; Upstill-Goddard and Barnes 2016). In addition, the shape of the CH_4 spatial profile in estuaries can be strongly modulated by the lateral inputs from intertidal areas (intertidal mudflats, saltmarshes, mangroves; Middelburg et al. 2002, Upstill-Goddard and Barnes 2016, Rosetrenter et al. 2018), creating peaks of CH_4 all along the estuary and not necessarily in the uppermost regions. However, these intertidal areas are reduced in microtidal lagoons and in strongly urbanized environments such as the JLC. Methanogenesis is a process of organic matter degradation that is favored when all the proton acceptors are depleted (i.e., nitrate, manganese, iron oxides, sulfate). High CH_4 concentrations are frequently found in water and wastewater of urban drainage systems composed of sewer systems, wastewater treatment plants, and receiving water bodies (Nirmal-Rajkumar et al. 2008; Yu et al. 2017). The primary methanogenic pathways are the conversion of acetate to CO_2 and CH_4 and reduction of CO_2 with H_2 (Whitman et al. 1992; Matson and Harriss 2009). In severely impacted estuaries, the CH_4 concentrations can span several orders of magnitude spatially and temporally (Nirmal-Rajkumar et al. 2008; Burgos et al. 2015; Cotovicz et al. 2016). The concentrations of dissolved CH_4 found in surface waters of JLC are very high, with an extreme maximum of 288,572 nmol L^{-1} in the river zone. To our best knowledge, this is the second highest concentration measured for any natural river-estuarine system, after that measured in the Adyar Estuary (maximum of 386,000 nmol L^{-1}; Nirmal-Rajkumar et al. 2008). The concentrations of CH_4 found in the polluted rivers of the JLC are also comparable to the lower ranges of CH_4 concentrations found in sewer systems (313,000 to 1,563,000 nmol L^{-1}; Guisasola et al. 2008, Foley et al. 2009). Taking into account the averaged dissolved CH_4 concentrations, the waters of JLC are also among the highest measured CH_4 concentrations worldwide (average of 976 nmol L^{-1}) and similar to strongly polluted estuaries such as the Adyar Estuary – India (2200 nmol L^{-1}; Nirmal-Rajkumar et al. 2008), Guadalete Estuary – Spain (590 nmol L^{-1}; Burgos et al. 2015), and Guanabara Bay – Brazil (456 nmol L^{-1}; Cotovicz et al. 2016). The anthropogenic-derived organic carbon in the JLC is likely to be massive, taking into account that the watershed hosts a huge population and the wastewater treatment covers less than 60% of the total households. The levels of accumulated precipitation were not correlated to the concentrations of CH_4; however, highest concentrations were observed in November 2017 (when the accumulated precipitation of 3 days before sampling was low), preventing the dilution by rainwater. Heavy rain events could occur in the region, with possibility to alter the CO_2 and CH_4 concentrations. Climatological and hydrological effects on GHG dynamics need further investigation.

There was a positive correlation between pCO_2 and CH_4 in all campaigns, suggesting a common source of these two gases (Fig. 6). However, for similar pCO_2 values, the concentrations of CH_4 spanned until one order of magnitude. This was also described in other estuaries, for example, in tropical mangrove-dominated estuaries of Australia, where the authors attributed this pattern to a combination of processes, including the presence of sewage treatment plants, differential groundwater and riverine carbon inputs, and exchange with vegetated coastal habitats (Rosetrenter et al. 2018). In the JLC, the presence of untreated domestic effluent discharges associated with

strong oxygen depletion seems to enhance disproportionally the production of CH_4 compared to CO_2, particularly during the sampling in November 2017. Another hypothesis that can explain these discrepancies in the peaks of CH_4 and of CO_2 is the inhibition of CH_4 oxidation in specific environmental conditions. The methanotrophy can be inhibited under high NH_4^+ concentrations (Bosse et al. 1993) or because the methanotroph community is outcompeted by other microbes such as nitrifiers. The reduction in CH_4 oxidation rates starts to be significant when the NH_4^+ concentrations are > 4000 μmol L^{-1} (Bosse et al. 1993). Indeed, the two highest measured CH_4 concentrations in JLC (sampling campaign in November 2017) are coincident with the highest NH_4^+ concentrations (> 5000 μmol L^{-1}) (Fig. 7). The two other sampling campaigns presented concomitant lower CH_4 and NH_4^+ concentrations, the latter being below the 4000 μmol L^{-1} threshold for the inhibition of CH_4 oxidation (Fig. 7). According to the analysis of Borges and Abril (2011) updated by Cotovicz et al. (2016), there is a positive relationship between CH_4 and pCO_2 in well-mixed estuarine systems and a marked negative relationship in stratified estuarine systems. In well-mixed systems, CH_4 and CO_2 present a positive tendency due to the degradation of allochthonous organic matter in soils and sediments that are then transported to the estuary, i.e., CO_2 and CH_4 present a same allochthonous origin. In stratified systems, the relationship is negative because the autochthonous organic matter is produced by primary producers in surface waters, consuming CO_2. The produced organic matter is further transferred across the pycnocline promoting anoxic conditions in bottom waters and sediments, favoring methanogenesis (Fenchel et al. 1995; Koné et al. 2010). The produced CH_4 is further transported to the surface water by diffusion and eventually bubble dissolution, turning the surface waters enriched in CH_4. However, these tendencies seem to be "perturbed" in anoxic and organic-rich coastal waters, when the CH_4 production is disproportionally favored. In addition, the inhibition of CH_4 oxidation under high NH_4^+ conditions seems to sustain the extremely high CH_4 concentrations in the JLC anoxic rivers, particularly in November 2017.

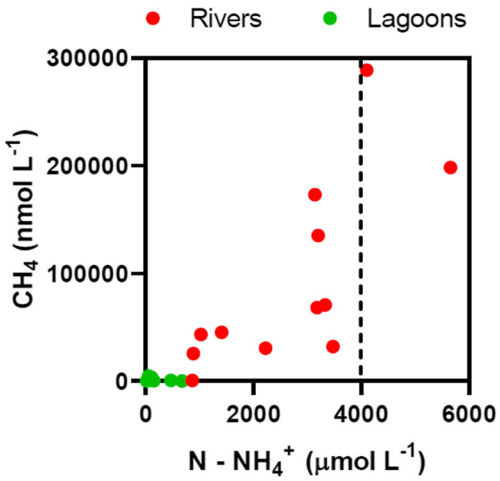

Fig. 7 Relationship between NH_4^+ vs. CH_4 dissolved concentrations in the JLC for the sampling campaigns in March 2017, June 2017, and November 2017. The red circles represent the river stations, whereas the green circles represent the lagoon stations. The vertical dotted line represents the theoretical threshold for NH4+ concentration (4000 μmol L^{-1}), above which the inhibition of CH_4 oxidation by NH_4^+ starts to be significant (Bosse et al. 1993)

Diffusive emissions of CO_2 and CH_4

According to the most recent global compilation of estuarine CO_2 emissions propose by Chen et al. (2013), upper estuaries are sources of CO_2 on the order of 106 mmol C m^{-2} d^{-1}, mid-estuaries emit 47 mmol C m^{-2} d^{-1}, and lower estuaries with salinities more than 25 are sources of 23 mmol C m^{-2} d^{-1}. Considering all JLC, the emissions ranged between 22.00 and 48.67 mmol m^{-2} d^{-1}. In this way, the CO_2 emissions in the JLC are within the range in other estuaries. However, considering only the river stations, CO_2 outgassing ranged between 199 and 435 mmol C m^{-2} d^{-1}, which is 2- to 4-fold higher than the averaged emissions of CO_2 by freshwaters and low-salinity regions of estuaries. Emissions of this order of magnitude were found only in high-impacted estuaries and carbon-rich environments, for example, in the Cochin Estuary – India (267 mmol C m^{-2} d^{-1}; Gupta et al. 2009); Douro, Elbe, Loire, Scheldt, and Sado estuaries – European estuaries (between 155 and 396 mmol C m^{-2} d^{-1}; Frankignoulle et al. 1998; Abril et al. 2003); Potou Lagoon – Ivory Coast (186.0 mmol C m^{-2} d^{-1}; Koné et al. 2009); and Tapti Estuary – India (362 mmol C m^{-2} d^{-1}; Sarma et al. 2012).

The air-water CH_4 fluxes to the atmosphere are strongly related to the typology of coastal ecosystems and also the degree of human influence. Concerning diffusion only, the air-water CH_4 fluxes range from 0.04 ± 0.17 mmol C m^{-2} d^{-1} for coastal plumes to 1.85 ± 0.99 mmol C m^{-2} d^{-1} for fjords and coastal lagoons, with intermediate values for low-salinity zones, marsh and mangrove creeks (Borges and Abril 2011). Considering the ecosystem as a whole, the JLC presented CH_4 emissions varying between 2.19 and 16.47 mmol m^{-2} d^{-1}, which are among the highest documented in estuaries worldwide (Bange 2006). The CH_4 emissions on this order of magnitude were found only in high-impacted ecosystems, for example, in the Adyar Estuary – India (4.70 mmol m^{-2} d^{-1}; Nirmal-Rajkumar et al. 2008), Coastal Lagoon of the Ivory Coast (2.40 mmol m^{-2} d^{-1}; Koné et al. 2010), and Guanabara Bay – Brazil (0.24 to 4.79 mmol m^{-2} d^{-1}; Cotovicz et al. 2016). The average flux intensities in the JLC are two to three orders of magnitude higher than values normally found in shelf waters (~0.03 mmol m^{-2} d^{-1}) and four to five orders of magnitude higher than values of the open ocean waters (~0.0004 mmol m^{-2} d^{-1}) (Borges et al. 2016).

We used the global warming potential (GWP) and CO_2-equivalent emissions (CO_2-eq) (IPCC 2013) to compare the

Table 4 Average values of CO_2 equivalent emissions (CO_2-eq) calculated for CO_2 and CH_4 degassing. The fluxes were calculated for "rivers" and "lagoons" stations, and after integrated for the entire superficial area, for each sampling campaign. The fluxes were calculated using the gas transfer velocity of Raymond and Cole (2001) (RC01)

	CO_2 emissions in CO_2-eq (g CO_2-eq m^{-2} d^{-1})	CH_4 emissions in CO_2-eq* (g CO_2-eq m^{-2} d^{-1})	Weight of CO_2 (%) (CO_2-eq)	Weight of CH_4 (%) (CO_2-eq)
March 2017				
Rivers (1.07 km^2)	27.47	29.40	48.30	51.70
Lagoons (12.08 km^2)	0.77	0.21	78.23	21.77
All system	2.94	2.58	53.21	46.79
area-weighted (13.15 km^2)				
June 2017				
Rivers	11.43	20.81	35.45	64.55
Lagoons	0.72	0.69	51.01	49.99
All system	1.48	2.17	40.51	59.49
area-weighted				
November 2017				
Rivers	10.73	67.20	13.77	86.23
Lagoons	0.26	0.62	29.42	70.58
All system	1.11	6.11	15.40	84.60
area-weighted				

* Fluxes of CH_4 multiplied by 28, which represents the GWP of CH_4 (IPCC 2013)

fluxes of CH_4 with those of CO_2. This metric was calculated with the gas transfer velocity of RC01, which provided intermediate values compared to the gas transfer velocity of W92 (lower range) and J08 (higher range). After converting to CO_2-eq, the emissions of CO_2 ranged between 1.11 and 2.94 g CO_2-eq m^{-2} d^{-1}. For CH_4, the CO_2-eq emissions ranged between 2.17 and 6.11 g CO_2-eq m^{-2} d^{-1} (Table 4). Expressed as CO_2-eq, CH_4 accounted for a major portion of the GHG warming potential in the lagoon (between 46 and 80%), especially in the river stations where the CH_4 was always more important than CO_2. This is an unusual case since CO_2 is generally the predominant GHG in aquatic coastal ecosystems (Campeau et al. 2014; Sadat-Noori et al. 2018). However, studies have suggested that CH_4 can be the main source of CO_2-eq emissions in small streams within the fluvial network and in mangrove ecosystems (Campeau et al. 2014; Sea et al. 2018). Here, we are showing that in extremely impacted ecosystem, CH_4 becomes a major contributor to GHG emission in terms of CO_2-eq. This study quantified only the diffusive emissions of CH_4; however, coastal areas ensure several pathways of CH_4 to the atmosphere, including the ebullition. The occurrence of CH_4 ebullition is highly probable in the JLC, since the threshold value of 5×10^4 nmol L^{-1} for dissolved CH_4 at which bubbles can form in aquatic sediments (Chanton et al. 1989) was regularly reached in the polluted rivers. Bubble evasion from the surface waters was visually observed in the river stations, which could make CH_4 contribution even stronger. In addition, bubble dissolution can occur during their travel through the water column, also contributing to the high CH_4 concentrations in the water and diffusive fluxes at the water-air interface (Martens and Klump 1980).

Conclusions

Our study reveals some of the biogeochemical processes that occur in tropical coastal lagoons receiving a discharge of strongly polluted rivers draining urban areas, with considerable impacts on carbonate chemistry and CO_2 and CH_4 emissions to the atmosphere. The rivers receive large amounts of anthropogenic-derived organic matter, mostly from domestic effluents, that are discharged "*in natura*" in the waters and present quasi-permanent oxygen depletion. In these freshwater areas of the lagoon, anaerobic processes such as denitrification and sulfate reduction are intrinsically coupled to a consumption of protons, which favor the production of TA. These oxic, suboxic, and anoxic processes contribute to the production of DIC in the form of excess of CO_2 and TA and strong production of CH_4. The calculated emissions of CO_2 and CH_4 in these polluted rivers are among the highest documented emissions in coastal waters.

In the lagoon stations at intermediate salinities, the deviation of chemical species from the conservative mixing reveals that additional processes are taking place along the river-ocean continuum. The concentrations of TA, DIC, CO_2, and CH_4 decreased substantially from the rivers to the lagoon waters. The decreases of TA and DIC are attributed to re-oxidation processes of inorganic reduces species such as sulfur, iron, and ammonia during the mixing of anoxic

freshwaters with oxic estuarine waters. The marked decreases of DIC concentrations are also attributed to CO_2 outgassing and phytoplanktonic primary production enhanced by a concomitant enrichment in nutrients. Although the lagoon waters remain most of the time oversaturated in CO_2, the growth of large phytoplankton blooms contributed occasionally to undersaturation, associated with high DO and pH. For CH_4, the seaward decrease was related to the mixing with seawater, degassing, and CH_4 oxidation. Considering only the lagoon stations, the CO_2 emissions were of the same order of magnitude than in other ecosystems worldwide; however, for CH_4, these emissions are among the highest reported yet.

When compared in terms of CO_2-eq, the CH_4 emissions were more important than those of CO_2, revealing that urban coastal ecosystems strongly polluted by anthropogenic-derived organic carbon and oxygen depleted produce more GHG in the form of CH_4 than CO_2. These results confirm that severely polluted and eutrophicated coastal lagoons are hotspots of GHG emissions. Therefore, global carbon budgets calculated for coastal regions must adequately integrate these hotspots in order to improve the reliability of the proposed estimates. In addition, urgent actions are needed with purposes to reduce the eutrophication in urban coastal ecosystems, in order to mitigate the climate change and to improve the ecosystem health.

Supplementary Information The online version contains supplementary material available at https://doi.org/10.1007/s11356-021-13362-2.

Acknowledgements This study was supported by the Carlos Chagas Foundation for Research Support of the State of Rio de Janeiro (FAPERJ; proc. no. E- 26202.785/2016) and by the Coordination for the Improvement of Higher Education Personnel (CAPES). Luiz C. Cotovicz Jr. thanks the Fundação Cearense de Apoio ao Desenvolvimento Científico e Tecnológico (FUNCAP; Proc. No. INT-00159-00009.01.00/19) and UFC-PRPPG for a visiting professor grant at the Marine Sciences Institute (LABOMAR). This work is also a contribution to the International Research Project *Vulnérabilité des Ecosystèmes Littoraux Tropicaux face à l'Eutrophisation* funded by the French National Centre for Scientific Research (CNRS-INEE); and a scientific contribution for the *Red Latinoamericana de Acidificación del Océano* (LAOCA).

Author contribution LCCJr: Conceptualization, Coordination, Execution, Data curation, Formal analysis, Methodology, Writing – original draft. RPR: Laboratorial Analysis, Writing – review. LOV, CRR, DT, LG: Execution, Laboratorial Analysis. MB, RS: Conceptualization, Execution, Writing – review. BAK: Conceptualization, Funding acquisition, Supervision, Writing – review. GA: Conceptualization, Data curation, Formal analysis, Methodology, Supervision, Writing – original draft.

Funding Carlos Chagas Foundation for Research Support of the State of Rio de Janeiro (FAPERJ; proc. no. E- 26202.785/2016).

Data availability The datasets used and/or analyzed during the current study are available from the corresponding author on reasonable request.

Declarations

Ethics approval and consent to participate Not applicable

Consent for publication Not applicable

Competing interests The authors declare no competing interests.

References

Abril G, Frankignoulle M (2001) Nitrogen – alkalinity interactions in the highly polluted Scheldt Basin (Belgium). Water Res 35:844–850. https://doi.org/10.1016/S0043-1354(00)00310-9

Abril G, Iversen N (2002) Methane dynamics in a shallow, non-tidal, estuary (Randers Fjord, Denmark). Mar Ecol Prog Ser 230:171–181. https://doi.org/10.3354/meps230171

Abril G, Etcheber H, Delille B, Frankignoulle M, Borges AV (2003) Carbonate dissolution in the turbid and eutrophic Loire estuary. Mar Ecol Prog Ser 259:129–138. https://doi.org/10.3354/meps259129

Abril G, Commarieu MV, Guerin F (2007) Enhanced methane oxidation in an estuarine turbidity maximum. Limnol Oceanogr 52:470–475. https://doi.org/10.4319/lo.2007.52.1.0470

Amarante, OA, Silva FJ, Rios Filho L G (2002) Wind power atlas of the Rio de Janeiro State. Secretaria de Estado da Energia da Indústria Naval e do Petróleo, Rio de Janeiro. (in Portuguese) http://www.cresesb.cepel.br/publicacoes/download/atlas_eolico/AtlasEolicoRJ.pdf. Accessed 27 April 2018

ANA 2019. Water National Agency. National atlas of sewage: depollution of river basins. (in Portuguese) http://www.snirh.gov.br/portal/snirh/snirh-1/atlas-esgotos. Accessed 25 January 2020

Baldry K, Saderne V, McCorkle D, Churchill JH, Agusti S, Duarte C (2019) Anomalies in the carbonate system of Red Sea coastal habitats. Biogeosciences 17:423–439. https://doi.org/10.5194/bg-17-423-2020

Bange HW (2006) Nitrous oxide and methane in European coastal waters. Estuar Coast Shelf Sci 70:361–374. https://doi.org/10.1016/j.ecss.2006.05.042

Beaulieu J, DelSontro T, Downing J (2019) Eutrophication will increase methane emissions from lakes and impoundments during the 21st century. Nat Commun 10:1–5. https://doi.org/10.1038/s41467-019-09100-5

Benson BB, Krause D (1984) The concentration and isotopic fractionation of oxygen dissolved in freshwater and seawater in equilibrium with the atmosphere. Limnol Oceanogr 29:620–632. https://doi.org/10.4319/lo.1984.29.3.0620

Borges AV, Abril G (2011) Carbon dioxide and methane dynamics in estuaries. In: McLusky D, Wolanski E (eds) Treatise on Estuarine and Coastal Science. Academic Press, Amsterdam, pp 119–161. https://doi.org/10.1016/B978-0-12-374711-2.00504-0

Borges AV, Gypens N (2010) Carbonate chemistry in the coastal zone responds more strongly to eutrophication than to ocean acidification. Limnol Oceanogr 55:346–353. https://doi.org/10.4319/lo.2010.55.1.0346

Borges AV, Champenois W, Gypens N, Delille B, Harlay J (2016) Massive marine methane emissions from near-shore shallow coastal areas. Sci Rep 6:27908. https://doi.org/10.1038/srep27908

Borges AV, Darchambeau F, Lambert T, Morana C, Allen GH, Tambwe E, Toengaho Sembaito A, Mambo T, Nlandu Wabakhangazi J,

Descy J-P, Teodoru CR, Bouillon S (2019) Variations in dissolved greenhouse gases (CO_2, CH_4, N_2O) in the Congo River network overwhelmingly driven by fluvial-wetland connectivity. Biogeosciences 16:3801–3834. https://doi.org/10.5194/bg-16-3801-2019

Bosse U, Frenzel P, Conrad R (1993) Inhibition of methane oxidation by ammonium in the surface layer of a littoral sediment. FEMS Microbiol Ecol 13:123–134. https://doi.org/10.1111/j.1574-6941.1993.tb00058.x

Bricker SB, Longstaff B, Dennison W, Jones A, Boicourt K, Wicks C, Woerner J (2008) Effects of nutrient enrichment in the nation's estuaries: a decade of change. Harmful Algae 8(623):21–32. https://doi.org/10.1016/j.hal.2008.08.028

Brigham BA, Bird JA, Juhl AR, Zappa CJ, Montero AD, O'Mullan GD (2019) Anthropogenic inputs from a coastal megacity are linked to greenhouse gas concentrations in the surrounding estuary. Limnol Oceanogr 64:2497–2511. https://doi.org/10.1002/lno.11200

Burgos M, Sierra A, Ortega T, Forja JM (2015) Anthropogenic effects on greenhouse gas (CH4 and N2O) emissions in the Guadalete River Estuary (SW Spain). Sci Total Environ 503–504:179–189. https://doi.org/10.1016/j.scitotenv.2014.06.038

Cai W-J, Pomeroy LR, Moran MA, Wang Y (1999) Oxygen and carbon dioxide mass balance for the estuarine–intertidal marsh complex of five rivers in the southeastern U.S. Limnol Oceanogr 44:639–649. https://doi.org/10.4319/lo.1999.44.3.0639

Cai W-J, Hu X, Huang W, Murrell MC, Lehrter JC, Lohrenz SE, Chou W, Zhai W, Hollibaugh JT, Wang Y, Zhao P, Guo X, Gundersen K, Dai M, Gong G (2011) Acidification of subsurface coastal waters enhanced by eutrophication. Nat Geosci 4:766–770. https://doi.org/10.1038/NGEO1297

Cai W-J, Huang W-J, Luther GW, Pierrot D, Li M, Testa J, Xue M, Joesoef A, Mann R, Brodeur J, Xu Y-Y, Chen B, Hussain N, Waldbusser GG, Cornwell J, Kemp WM (2017) Redox reactions and weak buffering capacity lead to acidification in the Chesapeake Bay. Nat Commun 8:369. https://doi.org/10.1038/s41467-017-00417-7

Campeau A, Lapierre J-F, Vachon D, del Giogio PA (2014) Regional contribution of CO_2 and CH_4 fluxes from the fluvial network in a lowland boreal landscape of Québec. Global Biogeochem Cy 28:57–69. https://doi.org/10.1002/2013GB004685

Chanton JP, Martens CS, Kelley CA (1989) Gas transport from methane saturated, tidal freshwater and wetland sediments. Limnol Oceanogr 34:807–819. https://doi.org/10.4319/lo.1989.34.5.0807

Chen CT, Huang TH, Chen YC, Bai Y, He X, Kang Y (2013) Air–sea exchanges of CO_2 in the world's coastal seas. Biogeosciences 10:6509–6544. https://doi.org/10.5194/bg-10-6509-2013

Cloern JE (2001) Our evolving conceptual model of the coastal eutrophication problem. Mar Ecol Prog Ser 210:223–253

Cotovicz LC, Knoppers BA, Brandini N, Costa Santos SJ, Abril G (2015) A strong CO_2 sink enhanced by eutrophication in a tropical coastal embayment (Guanabara Bay, Rio de Janeiro, Brazil). Biogeosciences 12:6125–6146. https://doi.org/10.5194/bg-12-6125-2015

Cotovicz LC, Knoppers BA, Brandini N, Poirier D, Costa Santos SJ, Abril G (2016) Spatio-temporal variability of methane (CH4) concentrations and diffusive fluxes from a tropical coastal embayment surrounded by a large urban area (Guanabara Bay, Rio de Janeiro, Brazil). Limnol Oceanogr 61:S238–S252. https://doi.org/10.1002/lno.10298

Cotovicz LC, Knoppers BA, Brandini N, Poirier D, Costa Santos SJ, Abril G (2018) Aragonite saturation state in a tropical coastal embayment dominated by phytoplankton blooms (Guanabara Bay - Brazil). Mar Pollut Bull 129:729–739. https://doi.org/10.1016/j.marpolbul.2017.10.064

Cotovicz LC, Vidal LO, de Rezende CE, Bernardes MC, Knoppers BA, Sobrinho RL, Cardoso RP, Muniz M, dos Anjos RM, Biehler A, Abril G (2020) Carbon dioxide sources and sinks in the delta of the Paraíba do Sul River (Southeastern Brazil) modulated by carbonate thermodynamics, gas exchange and ecosystem metabolism during estuarine mixing. Mar Chem 226:103869. https://doi.org/10.1016/j.marchem.2020.103869

De-Magalhães L, Noyma N, Furtado LL, Mucci M, van Oosterhout F, Huszar VLM, Marinho MM, Lürling M (2017) Efficacy of coagulants and ballast compounds in removal of cyanobacteria (Microcystis) from water of the tropical lagoon Jacarepaguá (Rio de Janeiro, Brazil). Estuar Coasts 40:121–133. https://doi.org/10.1007/s12237-016-0125-x

Dickson AG (1990) Standard potential of the reaction: AgCl(s) + $1/2H_2(g)$ = Ag(s) + HCl(aq), and the standard acidity constant of the ion HSO_4 in synthetic sea water from 273.15 to 318.15 K. J. Chem Thermodyn 22:113–127. https://doi.org/10.1016/0021-9614(90)90074-Z

Dickson AG, Millero FJ (1987) A comparison of the equilibrium constants for the dissociation of carbonic acid in seawater media. Deep-Sea Res 34:1733–1743. https://doi.org/10.1016/0198-0149(87)90021-5

Etheridge DM, Steele LP, Francey RJ, Langenfelds RL (1998) Atmospheric methane between 1000 A.D. and present: evidence of anthropogenic emissions and climatic variability. J Geophys Res 103:15979–15993. https://doi.org/10.1029/98JD00923

Fenchel T, Bernard C, Esteban G, Finlay BJ, Hansen PJ, Iversen N (1995) Microbial diversity and activity in a Danish Fjord with anoxic deep water. Ophelia 43(1):45–100

Foley J, Yuan Z, Lant P (2009) Dissolved methane in rising main sewer systems: field measurements and simple model development for estimating greenhouse gas emissions. Water Sci Technol 60:2963–2971. https://doi.org/10.2166/wst.2009.718

Frankignoulle M, Bourge I, Wollast R (1996) Atmospheric CO_2 fluxes in a highly polluted estuary (The Scheldt). Limnol Oceanogr 41:365–369. https://doi.org/10.4319/lo.1996.41.2.0365

Frankignoulle M, Abril G, Borges A, Bourge I, Canon C, Delille B, Libert E, Theate JM (1998) Carbon dioxide emission from European estuaries. Science 282:434–436. https://doi.org/10.1126/science.282.5388.434

Gomes AM, Sampaio P, Ferrão-Filho A, Magalhães VF, Marinho MM, Oliveira AC, Santos V, Domingos P, Azevedo SM (2009) Toxic cyanobacterial blooms in an eutrophicated coastal lagoon in Rio de Janeiro, Brazil: Effects on human health. Oecol Bras 13:329–345

Gran G (1952) Determination of the equivalence point in potentiometric titrations-part II. Analyst 77:661–671

Grasshoff K, Ehrhardt M, Kremling K (1999) Methods of seawater analysis, 3rd edn. Wiley-VCH, Weinhein

Guérin F, Abril G, Serça D, Delon C, Richard S, Delmas R, Tremblay A, Varfalvy L (2007) Gas transfer velocities of CO_2 and CH_4 in a tropical reservoir and its river downstream. J Mar Syst 66:161–172. https://doi.org/10.1016/j.jmarsys.2006.03.019

Guisasola A, de Hass D, Keller J, Yuan Z (2008) Methane formation in sewer systems. Water Res 42:1421–1430. https://doi.org/10.1016/j.watres.2007.10.014

Guo X, Dai M, Zhai W, Cai W-J, Chen B (2009) CO_2 flux and seasonal variability in a large subtropical estuarine system, the Pearl River Estuary, China. J Geophys Res 114:G03013. https://doi.org/10.1029/2008JG000905

Gupta GVM, Thottathil SD, Balachandran KK, Madhu NV, Madeswaran P, Nair S (2009) CO_2 supersaturation and net heterotrophy in a tropical estuary (Cochin, India): influence of anthropogenic effect. Ecosystems 12:1145–1157. https://doi.org/10.1007/s10021-009-9280-2

Gustafsson E, Hagens M, Sun X, Reed DC, Humborg C, Slomp CP, Gustafsson BG (2019) Sedimentary alkalinity generation and long-term alkalinity development in the Baltic Sea. Biogeosciences 16:437–456. https://doi.org/10.5194/bg-16-437-2019

Hammer MJ, Hammer MJ (2012) Water and wastewater technology. Prentice Hall, Pearson Education Inc, NJ, USA

Hu X, Cai W-J (2011) An assessment of ocean margin anaerobic processes on oceanic alkalinity budget. Global Biogeochem Cy 25: GB3003. https://doi.org/10.1029/2010GB003859

IPCC (2013) Climate change 2013: The physical science basis. Contribution of Working Group I to the Fifth Assessment Report of the Intergovernmental Panel on Climate Change. In: Stocker TF et al. (eds.) Cambridge Univ. Press. https://doi.org/10.1017/CBO9781107415324

Jähne B, Munnich KO, Bosinger R, Dutzi A, Huber W, Libner P (1987) On parameters influencing air-water exchange. J Geophys Res 92: 1937–1949. https://doi.org/10.1029/JC092iC02p01937

Jiang L-Q, Cai W-J, Wang Y (2008) A comparative study of carbon dioxide degassing in river- and marine-dominated estuaries. Limnol Oceanogr 53:2603–2615. https://doi.org/10.4319/lo.2008.53.6.2603

Kelley CA, Martens CS, Chanton JP (1990) Variations in sedimentary carbon remineralization rates in the White Oak River estuary, North Carolina. Limnol Oceanogr 35:372–383. https://doi.org/10.4319/lo.1990.35.2.0372

Kempe S (1990) Alkalinity: the link between anaerobic basins and shallow water carbonates? Naturwissenschaffer 7:426–427. https://doi.org/10.1007/BF01135940

Kjerfve B (1985) In: Wolfe DA (ed) Comparative oceanography of coastal lagoons. Academic, New York, pp 63–81

Knoppers BA, Carmouze JP, Moreira-Turcqo PF (1999) Nutrient dynamics, metabolism and eutrophication of lagoons along the east Fluminense coast, state of Rio de Janeiro, Brazil. In: Knoppers BA, Bidone ED, Abrão JJ (eds) Environmental geochemistry of coastal lagoon systems of Rio de Janeiro, Brazil. Programa de Geoquímica Ambiental, FINEP, UFF, Rio de Janeiro, pp 123–154

Koné YJM, Abril G, Kouadio KN, Delille B, Borges AV (2009) Seasonal variability of carbon dioxide in the rivers and lagoons of Ivory Coast (West Africa). Estuar Coasts 32:246–260. https://doi.org/10.1007/s12237-008-9121-0

Koné YJM, Abril G, Delille B, Borges AV (2010) Seasonal variability of methane in the rivers and lagoons of Ivory Coast (West Africa). Biogeochemistry 100:21–37. https://doi.org/10.1007/s10533-009-9402-0

Kubo A, Maeda Y, Kanda J (2017) A significant net sink for CO_2 in Tokyo Bay. Sci Rep 7:44355. https://doi.org/10.1038/srep44355

Lee K, Kim TW, Byrne RH, Millero FJ, Feely RA, Liu YM (2010) The universal ratio of boron to chlorinity for the North Pacific and North Atlantic oceans. Geochim Cosmochim Acta 74:1801–1811. https://doi.org/10.1016/j.gca.2009.12.027

Lorenzen C (1967) Determination of chlorophyll and pheo-pigments: spectrophotometric equations. Limnol Oceanogr 12:343–346. https://doi.org/10.4319/lo.1967.12.2.0343

Martens CS, Klump JV (1980) Biogeochemical cycling in an organic-rich coastal marine basin—I. Methane sediment– water exchange processes. Geochim Cosmochim Acta 44:471–490. https://doi.org/10.1016/0016-7037(80)90045-9

Martens CS, Albert DB, Alperin MJ (1998) Biogeochemical processes controlling methane in gassy coastal sediments—part 1. A model coupling organic matter flux to gas production, oxidation and transport. Cont Shelf Res 18:1741–1770. https://doi.org/10.1016/S0278-4343(98)00056-9

Matson PA, Harriss RC (2009) Biogenic trace gases: measuring emissions from soil and water. Blackwell Science, Oxford

McMahon PB, Dennehy KF (1999) N_2O emissions from a nitrogen enriched river. Environ Sci Technol 33:21–25. https://doi.org/10.1021/es980645n

Mehrbach C, Culberson CH, Hawley JE, Pytkowicz RM (1973) Measurements of the apparent dissociation constants of carbonic acid in seawater at atmospheric pressure. Limnol Oceanogr 18: 897–907. https://doi.org/10.4319/lo.1973.18.6.0897

Meybeck M, Ragu A (2012) GEMS-GLORI world river discharge database. Laboratoire de Géologie Appliquée, Université Pierre et Marie Curie, Paris, France, PANGAEA. https://doi.org/10.1594/PANGAEA.804574

Middelburg JJ, Nieuwenhuize J, Iversen N, Hoegh N, de Wilde H, Helder W, Seifert R, Christof O (2002) Methane distribution in European tidal estuaries. Biogeochemistry 59:95–119. https://doi.org/10.1023/A:1015515130419

Nirmal-Rajkumar A, Barnes J, Ramesh R, Purvaja R, Upstill-Goddard RC (2008) Methane and nitrous oxide fluxes in the polluted Adyar River and estuary, SE India. Mar Pollut Bull 56:2043–2051. https://doi.org/10.1016/j.marpolbul.2008.08.005

Nixon SW (1995) Coastal marine eutrophication: a definition, social causes, and future concerns. Ophelia 41:199–219. https://doi.org/10.1080/00785236.1995.10422044

NOAA (2019) National Oceanic and Atmospheric Administration. Earth System Research Laboratory. Global Monitoring Division. https://www.esrl.noaa.gov/gmd/ccgg/trends/monthly.html Accessed 20 June 2020

Rassmann J, Eitel EM, Lansard B, Cathalot C, Brandily C, Taillefert M, Rabouille C (2020) Benthic alkalinity and dissolved inorganic carbon fluxes in the Rhône River prodelta generated by decoupled aerobic and anaerobic processes. Biogeosciences 17:13–33. https://doi.org/10.5194/bg-17-13-2020

Raymond PA, Cole JJ (2001) Gas exchange in rivers and estuaries: choosing a gas transfer velocity. Estuaries 24:312–317. https://doi.org/10.2307/1352954

Reay DS, Smith P, Christensen TR, James RH, Clark H (2018) Methane and global environmental change. Annu Rev Environ Resour 43: 8.1–8.28. https://doi.org/10.1146/annurev-environ-102017-030154

Robbins LL, Hansen ME, Kleypas JA, Meylan SC (2010) CO_2 Calc: a user-friendly seawater carbon calculator for Windows, Max OS X, and iOS (iPhone), U.S. Geological Survey Open-File Report, 2010–1280, 1–17. http://pubs.usgs.gov/of/2010/1280/. Accessed 25 February 2019

Rosetrenter J, Maher DT, Erler DV, Murray R, Eyre BD (2018) Factors controlling seasonal CO_2 and CH_4 emissions in three tropical mangrove-dominated estuaries in Australia. Estuar Coast Shelf Sci 215:69–82. https://doi.org/10.1016/j.ecss.2018.10.003

Sadat-Noori M, Tait D, Maher D, Holloway C, Santos I (2018) Greenhouse gases and submarine groundwater discharge in a Sydney Harbour embayment (Australia). Estuar Coast Shelf Sci 31:499–509. https://doi.org/10.1016/j.ecss.2017.05.020

Salloto GRB, Cardoso AM, Coutinho FH, Pinto LH, Vieira RP, Chaia C, Lima JL, Albano RM, Martins OB, Clementino MM (2012) Pollution impacts on bacterioplankton diversity in a tropical urban coastal lagoon system. PLoS One 7:1–12. https://doi.org/10.1371/journal.pone.0051175

Samanta S, Dalai TK, Pattanaik JK, Rai SK, Mazumdar A (2015) Dissolved inorganic carbon (DIC) and its δ13C in the Ganga (Hooghly) River estuary, India: evidence of DIC generation via organic carbon degradation and carbonate dissolution. Geochem Cosmochim Acta 165:226–248. https://doi.org/10.1016/j.gca.2015.05.040

Sampaio GF (2008) Cianobactérias como parâmetros de qualidade ambiental: um estudo do Complexo Lagunar de Jacarepagua. Dissertation, Universidade do Estado do Rio de Janeiro

Santos Neves OM, Strauch JC, Ajara C (2017) Dasymetric methods applied to Jacarepagua watershed. Bull Geod Sci 23:606–622. https://doi.org/10.1590/S1982-21702017000400040

Sarma VVSS, Viswanadham R, Rao GD, Prasad VR, Kumar BSK, Naidu SA, Kumar NA, Rao DB, Sridevi T, Krishna MS, Reddy NPC, Sadhuram Y, Murty TVR (2012) Carbon dioxide emissions

from Indian monsoonal estuaries. Geophys Res Lett 39:L03602. https://doi.org/10.1029/2011GL050709

Sea M, Garcias-Bonet N, Saderne V, Duarte C (2018) Carbon dioxide and methane fluxes at the air–sea interface of Red Sea mangroves. Biogeosciences 15:5365–5375. https://doi.org/10.5194/bg-15-5365-2018

Siegenthaler U, Stocker TF, Monnin E, Lüthi D, Schwander J, Stauffer B, Raynaud D, Barnola JM, Fischer H, Masson-Delmotte V, Jouzel J (2005) Stable carbon cycle–climate relationship during the late Pleistocene. Science 25:1313–1317. https://doi.org/10.1126/science.1120130

Sunda WG, Cai W-J (2012) Eutrophication induced CO_2-acidification of subsurface coastal waters: interactive effects of temperature, salinity, and atmospheric PCO_2. Environ Sci Technol 46:10651–10659. https://doi.org/10.1021/es300626f

Thomas H, Schiettecatte L, Suykens K, Kon YJM (2009) Enhanced ocean carbon storage from anaerobic alkalinity generation in coastal sediments. Biogeosciences 6:267–274. https://doi.org/10.5194/bg-6-267-2009

Upstill-Goddard RC, Barnes J (2016) Methane emissions from UK estuaries: re-evaluating the estuarine source of tropospheric methane from Europe. Mar Chem 180:14–23. https://doi.org/10.1016/j.marchem.2016.01.010

Upstill-Goddard RC, Barnes J, Frost T, Punshon S, Owens NJP (2000) Methane in the Southern North Sea: low salinity inputs, estuarine removal and atmospheric flux. Global Biogeochem Cy 14:1205–1217. https://doi.org/10.1029/1999GB001236

Wallace YM (2005) Guidelines for estimating sewage flows for sewage infrastructure planning. Technical Report No.: EPD/TP 1/05. Environmental Protection Department. Hong Kong. https://www.epd.gov.hk/epd/sites/default/files/epd/english/environmentinhk/water/guide_ref/files/gesf.pdf Accessed 10 March 2019

Wanninkhof R (1992) Relationship between gas exchange and wind speed over the ocean. J Geophys Res 97:7373–7382. https://doi.org/10.1029/92JC00188

Weiss RF (1974) Carbon dioxide in water and seawater: the solubility of a non-ideal gas. Mar Chem 2:203–215. https://doi.org/10.1016/0304-4203(74)90015-2

Whitman WB, Bowen TI, Boone DR (1992) The methanogenic bacteria. In: Barlows A, Truper HG, Dworkin M, Harder W, Schleifer KH (eds) The prokaryotes, 2nd edn. Springer-Verlag, New York

Wolf-Gladrow DA, Zeebe RE, Klaas C, Körtzinger A, Dickson AG (2007) Total alkalinity: the explicit conservative expression and its application to biogeochemical processes. Mar Chem 106:287–300. https://doi.org/10.1016/j.marchem.2007.01.006

Xu Y-Y, Pierrot D, Cai W-J (2017) CO2 SYS Ocean carbonate system computation for anoxic waters using an updated CO2SYS program. Mar Chem 195:90–93. https://doi.org/10.1016/j.marchem.2017.07.002

Yamamoto S, Alcauskas JB, Crozier TE (1976) Solubility of methane in distilled water and seawater. J Chem Eng Data 21:78–80. https://doi.org/10.1021/je60068a029

Yu Z, Wang D, Li Y, Deng H, Hu B, Ye M, Zhou X, Da L, Chen Z, Xu S (2017) Carbon dioxide and methane dynamics in a human-dominated lowland coastal river network (Shanghai, China). J Geophys Res Biogeosci 122:1738–1758. https://doi.org/10.1002/2017JG003798

Zhai W, Dai M, Guo X (2007) Carbonate system and CO_2 degassing fluxes in the inner estuary of Changjiang (Yangtze) River, China. Mar Chem 107:342–356. https://doi.org/10.1016/j.marchem.2007.02.0